Supercooled and glassy water

2003 J. Phys.: Condens. Matter 15 R1669

(http://iopscience.iop.org/0953-8984/15/45/R01)

INSTITUTE OF PHYSICS PUBLISHING JOURNAL OF PHYSICS: CONDENSED MATTER

J. Phys.: Condens. Matter **15** (2003) R1669–R1726 PII: S0953-8984(03)21725-2

TOPICAL REVIEW

Supercooled and glassy water

Pablo G Debenedetti

Department of Chemical Engineering, Princeton University, Princeton, NJ 08544, USA

E-mail: pdebene@princeton.edu

Received 5 September 2003
Published 31 October 2003
Online at stacks.iop.org/JPhysCM/15/R1669

Abstract

The anomalous properties of cold and supercooled water, such as the fact that at sufficiently low temperatures it becomes more compressible and less dense when cooled, and more fluid when compressed, have attracted the attention of physical scientists for a long time. The discovery in the 1970s that several thermodynamic and transport properties of supercooled water exhibit a pronounced temperature dependence and appear to diverge slightly below the homogeneous nucleation temperature inspired a large number of experimental and theoretical studies. Likewise, an important body of work on glassy water has been stimulated by experiments, starting in the mid-1980s and continuing to this date, which suggest that vitreous water can exist in at least two apparently distinct forms. A coherent theory of the thermodynamic and transport properties of supercooled and glassy water does not yet exist. Nevertheless, significant progress towards this goal has been made during the past 20 years. This article summarizes the known experimental facts and reviews critically theoretical and computational work aimed at interpreting the observations and providing a unified viewpoint on cold, non-crystalline, metastable states of water.

Contents

1. Introduction

Water affects virtually every aspect of our lives, from climate to travel and from agriculture to public health. Its properties have a profound influence on the physical and chemical processes that are essential for life [1]. It is difficult to think of an industrial process that does not involve water as a solvent, product, reactant, or as an impurity. As one of the Aristotelian elements, water has long been central to scientific thought [2, 3]. Countless masterpieces in music, painting, architecture, and literature attest to water's central place in our collective imagination [2].

To the modern physical scientist water is a source of fascination on account of its unusual properties. It is the only chemical compound that occurs naturally in the solid, liquid and vapour phases, and the only naturally occurring inorganic liquid on earth [1]. Cold liquid water expands and becomes more compressible when cooled, and less viscous when compressed. Its dielectric constant in the normal liquid range is unusually large, and its melting and boiling temperatures are uncommonly high for a non-metallic hydride. In the crystalline state, water has thirteen known polymorphs, of which nine (ices II, III, V, VI, VII, VIII, X, XI and ordinary hexagonal ice, Ih) are stable over a certain range of temperature and pressure, and four are metastable (ices IV, IX, XII and cubic ice, Ic) [4, 5]. Liquid water's anomalies become more pronounced when it is cooled below the freezing point without crystallizing (supercooled). In fact water's oddities at ambient conditions, such as the fact that it becomes less compressible when heated, are remnants of more pronounced low-temperature anomalies. It is therefore necessary to investigate water in the supercooled range in order to fully understand its properties at ambient conditions. Many thermophysical properties of supercooled water exhibit a pronounced temperature dependence. When these properties are extrapolated slightly beyond the limit where ordinary measurements are no longer possible because of homogeneous nucleation of the stable crystalline phase, they appear to diverge. Understanding the origin of this behaviour is a major scientific challenge.

The two decades since the publication of Angell's classic review articles on supercooled water [6, 7] have witnessed intense research activity on the amorphous solid (glassy) forms of water. When cooled fast enough to avoid crystallization, water, like other liquids, vitrifies. Unlike most other substances, though, glassy water can apparently exist in at least two distinct forms, of which one pair may be separated by a first-order phase transition. One of the most important ideas of the past two decades in this field is the realization that supercooled and glassy water are intimately related, and that fundamental understanding of metastable water

must encompass both its liquid and vitreous states. The purpose of this article is to summarize the experimental facts and to review theoretical progress towards a comprehensive picture of the thermodynamic and transport properties of supercooled and glassy water.

Space constraints and thematic unity necessarily impose limits on the scope of any review. The present one being no exception, important topics such as supercooling and vitrification in aqueous solutions (e.g., [8]) and supercooling and vitrification of water in restricted geometries (e.g., [9–11]) are not discussed.

2. The water molecule and hydrogen bonds

The water molecule consists of two hydrogen atoms and an oxygen atom. The HOH angle is 104.5°, and the intramolecular OH distance is 0.957 Å [12]. The partial charges on the oxygen and hydrogen atoms and their mutual geometrical arrangement give rise to a dipole moment of 1.84 D in the vapour phase. If the OH bonds were fully ionic, the dipole moment would be 5.61 D. Each OH bond is therefore approximately $1/3$ ionic and $2/3$ covalent in character [13].

A strong, directional attraction can occur between an oxygen atom and a hydrogen atom belonging to a different water molecule. When this happens, a hydrogen bond is said to exist [14]. Ordinary hexagonal ice (Ih), the stable form of water below 273 K at atmospheric pressure, constitutes the best-known example of the water molecule's ability to engage in multiple hydrogen bonds. Each water molecule in ice has four nearest neighbours, and acts as a hydrogen donor to two of them, and as hydrogen acceptor to the other two. There results a space-filling network in which these four nearest neighbours are located at the vertices of a regular tetrahedron surrounding the central oxygen atom, and each O–O distance is 2.74 Å. The HOH angle in the water molecule is very close to the tetrahedral angle, 109.5°. The tetrahedrally coordinated network of ice is held together by hydrogen bonds. On account of the strong directionality of the bonds, the network is open. When ice melts at atmospheric pressure, loss of long-range order is accompanied by a 9% density increase. The strength of a hydrogen bond is approximately 20 kJ mol^{-1}, that is to say, some 8 kT at ambient temperature. This is considerably stronger than a regular dispersive interaction, about 1 kJ mol^{-1}, but significantly weaker than a covalent bond, about 400 kJ mol^{-1}. The heat of fusion of ice Ih at atmospheric pressure is 6.01 kJ mol^{-1}, and the heat of sublimation at the triple point is 51.09 kJ mol^{-1} [12]. This implies that the majority of hydrogen bonds are unbroken upon melting. Thus, in liquid water close to the melting point, and more so in supercooled water, local tetrahedral symmetry persists, although this order is transient and short-ranged.

The origin of water's unusual properties is the tendency of molecules to attract each other strongly through hydrogen bonds [13]. This added energetic stability is achieved by forming transient tetrahedral arrangements in which bond strength and directionality impose a low local density and cause a loss of orientational entropy. At sufficiently low temperatures, therefore, hydrogen bonds force energy and volume, as well as entropy and volume, to be negatively correlated. In most other liquids these correlations are positive.

3. Water in the stable liquid range

In order to discuss the behaviour of supercooled water, it is useful first to review some of the properties of water in the stable liquid range. The isobaric heat capacity of liquid water at atmospheric pressure is approximately 76 J mol^{-1} K^{-1}. It exhibits a weak minimum with respect to temperature at 35 °C, changes by less than 1% across the stable liquid range, and is reduced to

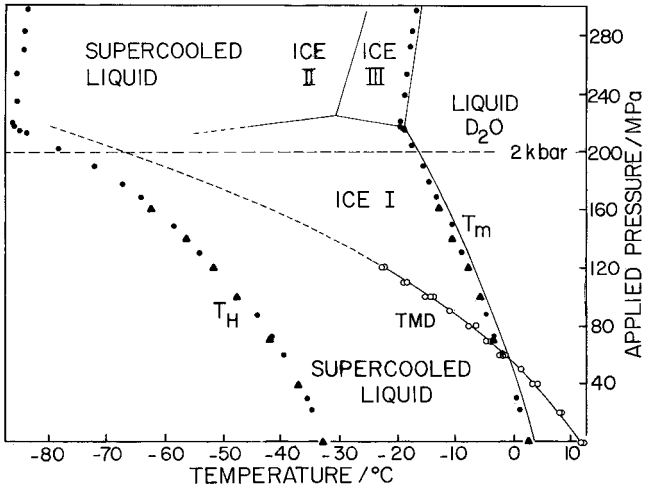

Figure 1. The TMD for D_2O as a function of pressure: experimental (○); and extrapolated from [310] (— · —). T_M is the melting temperature, and T_H is the homogeneous nucleation locus (see also section 4). Reprinted, with permission, from [63] Angell C A and Kanno H 1976 *Science* **193** 1121. Copyright (1976) AAAS.

approximately half its liquid-phase value upon boiling or freezing [1]. The isochoric heat capacity decreases monotonically across the melting-to-boiling range: it equals 75.9 J mol^{-1} K^{-1} for the liquid at the triple point, and 67.9 J mol^{-1} K^{-1} at the boiling point [15].

The specific volume of water decreases by 1.621 cm^3 mol^{-1}, or 8.3%, to 18.0182 cm^3 mol^{-1}, upon melting at 1 bar [12]. It decreases further with increasing temperature, reaching a minimum of 18.0158 cm^3 mol^{-1} at 4 °C, and increases monotonically thereafter, to 18.798 cm^3 mol^{-1} at the boiling point [12]. Although the magnitude of this effect is small, it has important thermodynamic consequences. The locus of temperatures at which the density is maximum at fixed pressure defines water's locus of density maxima, also referred to as the temperature of maximum density (TMD). At positive pressure this locus has a negative slope in the (P, T) plane; see figure 1. The following thermodynamic identity relates the slope of the TMD to the temperature dependence of the isothermal compressibility K_T [16]:

$$\left(\frac{\partial K_T}{\partial T}\right)_{P,\text{at TMD}} = \frac{v^{-1}(\partial^2 v/\partial T^2)_{P,\text{at TMD}}}{(\mathrm{d}p/\mathrm{d}T)_{\text{TMD}}} \tag{1}$$

where $K_T = -(\partial \ln v/\partial P)_T$, v is the molar volume, the subscript 'at TMD' signifies that the partial derivative is evaluated at a point on the TMD locus, and the subscript TMD signifies that the derivative is evaluated along the TMD locus, at the state point of interest. The numerator of the right-hand side is positive at the TMD [16]. Equation (1) therefore shows that a negatively sloped TMD necessarily implies that the compressibility must increase upon cooling. A pronounced increase in compressibility upon cooling is a distinguishing feature of supercooled water.

When a liquid is superheated, that is to say heated above the boiling point without boiling, its compressibility increases. Furthermore, the isothermal compressibility of any fluid is infinite at the critical point. It follows that, at any sub-critical pressure, the isothermal compressibility of a liquid is an increasing function of temperature near the vapour–liquid coexistence region. Water's well-known isothermal compressibility minimum (figure 2) is

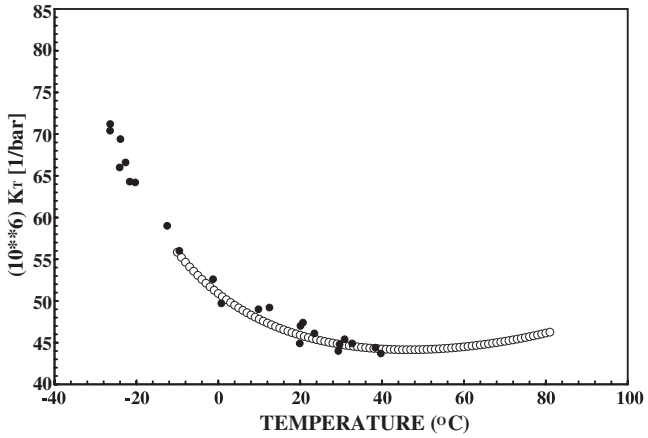

Figure 2. The temperature dependence of water's isothermal compressibility K_T at atmospheric pressure. Note the minimum at 46 °C. A multiparameter fit of the data for stable and moderately supercooled water from [311] (○). Also shown are the scanned and digitized supercooled water measurements of Speedy and Angell [60] (●).

therefore a direct consequence of the existence of a TMD, and signals the particular pressure-dependent temperature where $(\partial K_T/\partial T)_P$ changes sign. The low-temperature region where $(\partial K_T/\partial T)_P$ is negative reflects the influence of the TMD; the high-temperature region where this quantity is positive reflects the influence of the superheated liquid spinodal.

Water's thermal expansion coefficient α $(=(\partial \ln v/\partial T)_P)$ is negative below 4 °C at atmospheric pressure. Since the TMD locus is the boundary between states where $\alpha > 0$ and those where this quantity is negative, it follows from figure 1 that water's thermodynamic anomalies are suppressed upon compression and heating. This can also be seen from the thermodynamic identity

$$\left(\frac{\partial K_T}{\partial T}\right)_P = -\left(\frac{\partial \alpha}{\partial P}\right)_T. \tag{2}$$

Together with equation (1) and figure 1 the above equation implies that the magnitude of α decreases upon compression in the large part of the anomalous region ($\alpha < 0$) where the left-hand side of equation (2) is negative.

A salient characteristic of water's behaviour at atmospheric pressure is the fact that its response functions (response of density or entropy to changes in temperature or pressure) increase in magnitude upon cooling [3]. This increase starts at 46 °C for the compressibility, 35 °C for the isobaric heat capacity c_p $(= T^{-1}(\partial s/\partial T)_P)$ and 4 °C for the coefficient of thermal expansion, and becomes more pronounced as the temperature lowers. Each of the response functions is associated with a corresponding fluctuation [17]

$$\langle(\delta V)^2\rangle = VkTK_T \tag{3a}$$

$$\langle(\delta S)^2\rangle = Nkc_p \tag{3b}$$

$$\langle(\delta S\,\delta V)\rangle = VkT\alpha. \tag{3c}$$

The compressibility is a measure of volume fluctuations (V being the mean value of the fluctuating volume for a fixed number of molecules). The isobaric heat capacity is proportional to the entropy fluctuations experienced by N molecules at fixed pressure. The thermal expansion coefficient reflects the correlations between entropy and volume fluctuations (V being the mean value of the fluctuating volume for a fixed number of molecules). In most

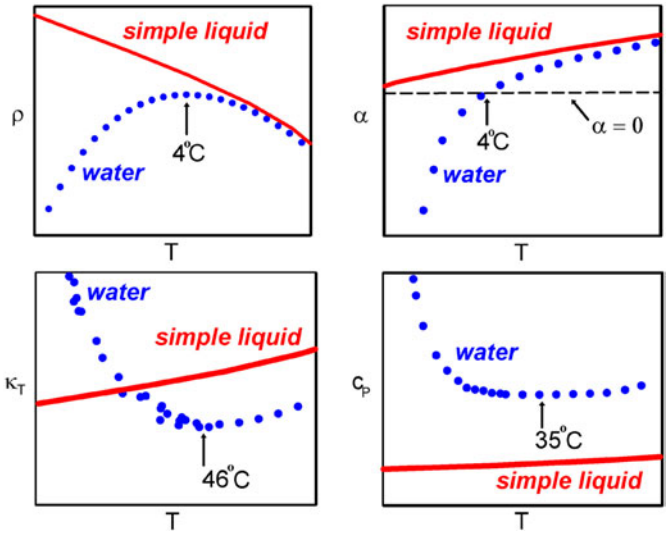

Figure 3. A schematic comparison of the isobaric temperature dependence of the density ρ, thermal expansion coefficient α, isothermal compressibility K_T and isobaric heat capacity c_p for water and a simple liquid.

(This figure is in colour only in the electronic version)

liquids, volume and entropy fluctuations become smaller as the temperature decreases. In water, on the other hand, volume and entropy fluctuations become more pronounced as the temperature lowers. In most liquids, entropy and volume fluctuations are positively correlated: an increase in volume results in a corresponding increase in entropy. In water below 4 °C, on the other hand, volume and entropy fluctuations are anti-correlated: a decrease in volume brings about an increase in entropy. Figure 3 illustrates the striking contrast between water and 'normal' liquids. This dichotomy becomes increasingly pronounced in the supercooled range.

The anti-correlation between entropy and volume is a consequence of the formation of an open hydrogen bonded network, in which a decrease in orientational entropy is accompanied by a volume increase. Although this network is transient and short-ranged in the liquid, as opposed to being permanent and long-ranged in ice, it is the microscopic basis for water's negative thermal expansion, and consequently it influences the thermodynamics of liquid water profoundly.

At temperatures between 273 and 306 K, the shear viscosity of liquid water decreases with pressure up to about 1 kbar (figure 4) [1, 18]. Likewise, the self-diffusion coefficient increases with pressure for temperatures lower than 300 K [19]. The pressure dependence of these transport coefficients is anomalous: in most liquids, compression causes loss of fluidity. In cold water, on the other hand, compression disrupts the hydrogen bond network, giving rise to increased fluidity [20, 21]. Translating this qualitative physical picture into a predictive theory for water's transport properties remains, as with thermodynamic quantities, a major challenge.

4. Ranges of stability and metastability

Figure 5 shows the temperature domains of stability and metastability for liquid and glassy water at atmospheric pressure [3, 22]. The stable liquid range is limited by the

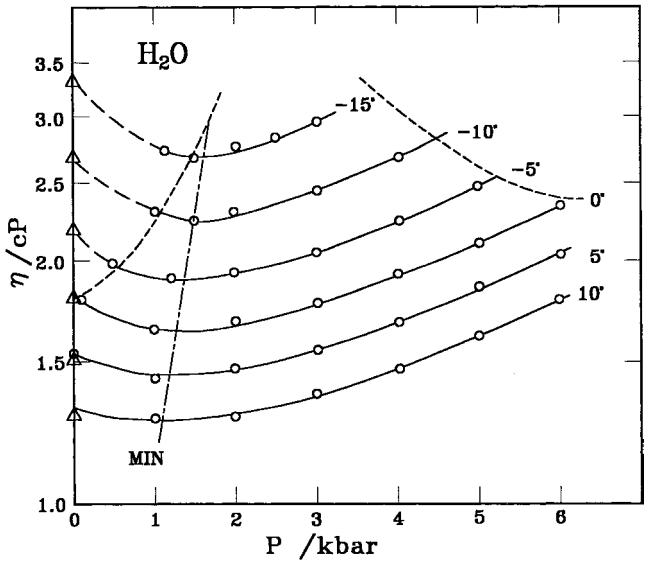

Figure 4. The pressure dependence of the shear viscosity of water. The dashed lines are phase boundaries (ice Ih, left; ice V, right). The locus of minima is also shown. Reprinted, with permission, from [24], Debenedetti P G, *Metastable Liquids, Concepts and Principles* copyright (1996) Princeton University Press, and adapted originally from [18].

equilibrium melting (0 °C) and boiling points (100 °C). Water can be superheated up to about 280 °C [23, 24], although an even higher temperature, 302 °C, has been reported in a pulse heating experiment [25]. Small droplets, with diameters in the 1–10 μm range, can be supercooled down to about −42 °C [24, 26, 27]. This range (−42 to 280 °C) is more than three times wider than the stable liquid range. Glassy water formed by rapid cooling of the liquid has a glass transition temperature of about 136 K [28, 29]. Recently, it has been argued that this temperature should be re-assigned to 165 K [8, 30] (glassy water is discussed in section 6). When vitreous water is heated, it crystallizes spontaneously to ice Ic (cubic ice) at around 150 K [28, 31].

In water, as in any other liquid, the onset of crystallization can be shifted to lower temperatures by reducing the concentration of nucleation-inducing impurities. This is usually done by purifying the sample and subdividing it into small droplets [32–36]. If the concentration of crystallization-inducing impurities is reduced to, say, 10^{12} l^{-1}, a 5 μm droplet will, on average, contain less than one impurity [6]. Such droplets can be easily supercooled down to a temperature where the intrinsic rate of crystallization becomes so large that the lifetime of the droplet becomes vanishingly small: the lifetime of a 5 μm droplet under conditions where the nucleation rate reaches 10^{15} cm^{-3} s^{-1}, for example, is 10^{-5} s. This condition defines a pressure-dependent experimentally attainable 'limit' of supercooling, commonly referred to as the homogeneous nucleation temperature. Because of the extraordinary sensitivity of the nucleation rate to the extent of supercooling [24], the attainable limit of supercooling is a weak (logarithmic) function of droplet diameter.

The above-defined conditions (1–10 μm droplets exposed to sub-freezing temperatures and free of ice-nucleating impurities) occur naturally in cirrus clouds, where liquid water below −40 °C has been observed [24, 37, 38]. More recent observations have demonstrated the existence of large quantities of liquid water down to −37.5 °C in deep convective clouds [39].

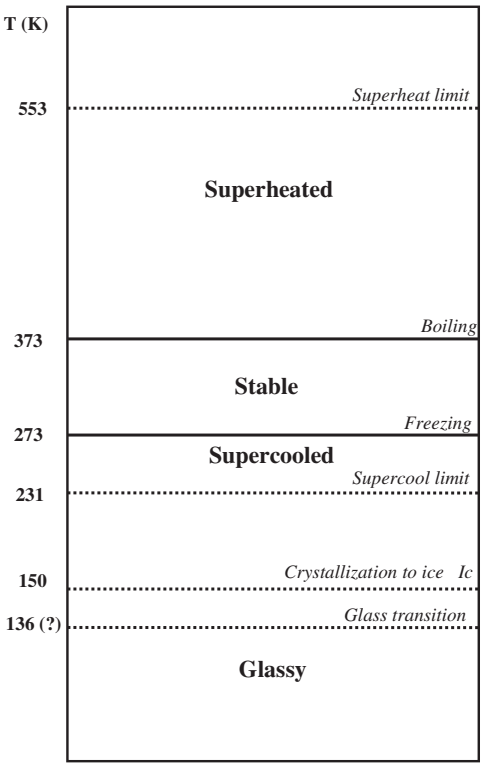

Figure 5. Temperature domains of stability and metastability for liquid and glassy water at atmospheric pressure. Equilibrium transitions are shown as full lines, kinetically controlled transitions as dotted lines. Adapted from [3] and [22].

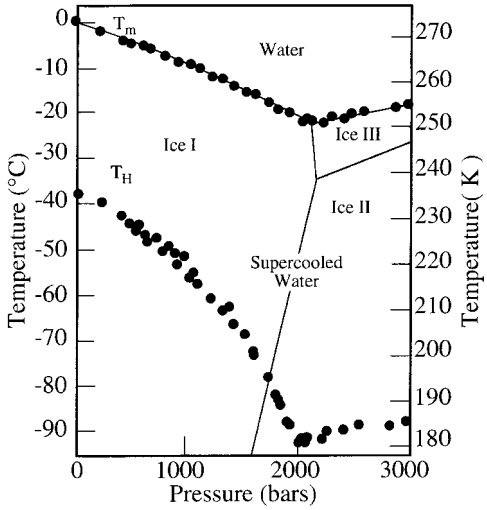

Figure 6. Homogeneous nucleation temperature of water droplets emulsified in a liquid hydrocarbon continuum phase as a function of pressure (T_H). T_M is the melting temperature. Reprinted, with permission, from [24], Debenedetti P G, *Metastable Liquids, Concepts and Principles* copyright (1996) Princeton University Press, and adapted originally from [33].

These studies highlight the importance of supercooled water in cloud processes such as rainfall and electrification [40–42].

Water's homogeneous nucleation limit is shown in figure 6. These experiments were performed using water-in-oil emulsions stabilized by sorbitan tristearate (surfactant), with either *n*-heptane or mixtures of methylcyclopentane and methylcyclohexane as the continuous phase, and water droplet sizes in the 1–10 μm range [33]. At atmospheric pressure water can be supercooled to about $-42\,^{\circ}$C [26, 27]. The homogeneous nucleation temperature reaches a minimum of $-92\,^{\circ}$C at 2 kbar. The parallelism between the homogeneous nucleation and melting loci is indicative of a corresponding change in the nature of the solid phase formed by the nucleation process.

Because of the spectacular increase in the nucleation rate and the consequent decrease of droplet lifetime, the roughly 80 K wide interval between the homogeneous nucleation temperature and the spontaneous crystallization to ice Ic is sometimes regarded as a region where liquid water cannot be observed ('no man's land' [22]). It should be remembered, however, that the homogeneous nucleation temperature is a kinetic constraint, not a thermodynamic one. Hence it is not an absolute but a practical limit, and is a function of the cooling rate and the observation time. The very fact that glassy water can be formed by

rapid cooling means that it is possible to cool water faster than it crystallizes, and homogeneous nucleation can be bypassed. The challenge is then to make measurements in the very short times available during rapid cooling, when water is still liquid. An important step in this direction has been taken by Bartell [43, 44]. He used evaporative cooling of molecular clusters produced by condensation of water vapour in supersonic flow through small nozzles. Typical cluster sizes and cooling rates were 74 Å (6600 molecules), and 10^7 K s^{-1}, respectively. Electron diffraction patterns of the water clusters showed no evidence of crystallization until roughly 200 K, whereupon freezing to ice Ic occurred (the cluster temperatures and hence the cooling rates were calculated, not measured, in these experiments). Also noteworthy are small-angle neutron scattering (SANS) measurements on supercooled D_2O droplets (5–8 nm) produced by expansion of a N_2–D_2O mixture in a Laval nozzle [45]. Calculated temperatures as low as 210 K were reported for liquid droplets in these experiments [45]. The SANS measurements allow the characterization of droplet size, and the technique has been applied both to pure D_2O [45, 46] and H_2O–D_2O mixtures [47, 48].

These supersonic flow experiments demonstrate that it is possible to make measurements on liquid water below $-42\,^{\circ}$C. This requires sample sizes smaller than the customary micrometre range, very fast cooling and considerable experimental ingenuity in carrying out thermophysical property measurements over very short time windows. But these are not insurmountable obstacles. Experimental studies of liquid water below the homogeneous nucleation 'limit' are not only possible but urgently needed for a definitive picture of the thermodynamics of supercooled water. An important degree of freedom not exploited to date is the fact that the rate of nucleation in water, as in all supercooled liquids, is a non-monotonic function of temperature. This is a consequence of the competition between increase in the thermodynamic driving force and viscous slow-down upon supercooling, giving rise to sharp extrema in the temperature dependence of nucleation rates [24]. This means that although rapid cooling is needed to bypass crystallization, there exists a range of temperatures below the homogeneous nucleation 'limit' within which droplet lifetimes increase with further cooling. Diffusion measurements in the range 150 K $< T <$ 160 K [49], and measurements of flow properties at 140 K [50] suggest rich experimental possibilities in the temperature range where water, after being rapidly cooled, is hot enough to be no longer a glass, but cold enough to not yet crystallize at a measurable rate [51].

5. Properties of supercooled water

5.1. Density and its derivatives

Table 1 lists experimental measurements of supercooled water's density, its temperature and pressure derivatives (i.e., thermal expansion coefficient and isothermal compressibility, respectively), and its TMD.

At atmospheric pressure the density of supercooled water decreases with decreasing temperature (figure 7). The isothermal compressibility and the magnitude of the thermal expansion coefficient increase markedly with decreasing temperature (figures 2 and 8). Application of pressure (figures 9 and 10) displaces the anomalies to lower temperatures. As shown by equations (1) and (2), thermodynamic consistency dictates that the increase in isothermal compressibility upon isobaric cooling and the decrease in the magnitude of the negative thermal expansion coefficient upon isothermal compression are inseparable from the existence of a negatively sloped TMD, such as water possesses at the conditions where it has been measured.

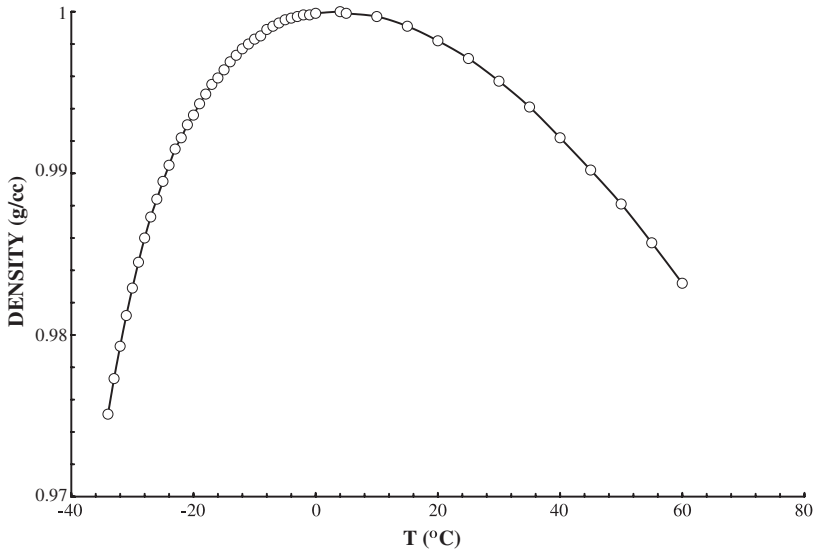

Figure 7. The temperature dependence of liquid water's density at atmospheric pressure. Data from [54] (−34 to 4 °C) and [312] (5–60 °C).

Table 1. Measurements of supercooled water's density and its derivatives.

Property	Range[a]	Reference
Density, thermal expansion coefficient	1 bar; −23/4 °C	[52]
	1 bar; −40/24 °C	[53]
	1 bar; −34(H), −29(D)/4 °C	[54]
	1 bar; −35(H), −30(D)/5 °C	[55]
	1/1500 bar; −26/20 °C(D)	[56][b,c]
	1 bar; −34(H), −19(D)/40 °C	[57][b]
	1 bar; −33/−5 °C	[58][b]
	1/2000 bar; −20/25 °C	[59][b,d]
Isothermal compressibility	1 bar; −26/45 °C	[60]
	1/1900 bar; −30/25 °C (H&D)	[61]
	1 bar; −34/25 °C	[62]
Temperature of maximum density	1/1200 bar; −24/15 °C(D)	[63]
	−230/1 bar; 6/14 °C (H&D)	[64]

[a] $H = H_2O$; $D = D_2O$. Measurements are for H_2O unless otherwise indicated.
[b] Thermal expansion coefficient tables or graphs also provided.
[c] Temperature of maximum density tables or graphs also provided.
[d] Isothermal compressibility tables or graphs also provided.

5.2. Heat capacity

Table 2 lists experimental measurements of supercooled water's isobaric heat capacity.

At atmospheric pressure the isobaric heat capacity of supercooled water increases markedly with decreasing temperature (figure 11). The more recent bulk measurements due to Tombari *et al* [70] show an even more pronounced decrease. To date, equivalent measurements at high pressure have not been done. The isochoric heat capacity, c_v, has been measured at

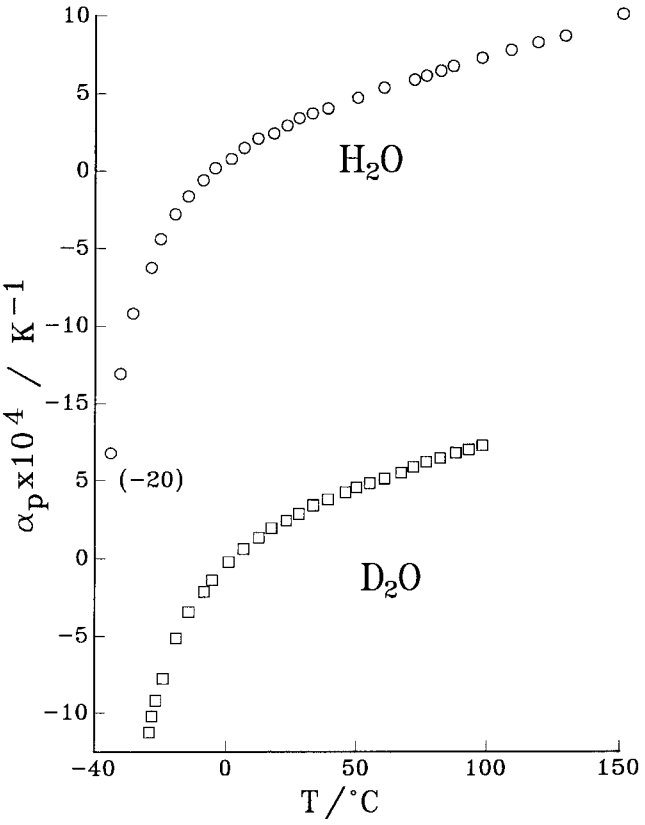

Figure 8. The temperature dependence of the thermal expansion coefficient of supercooled H_2O and D_2O at atmospheric pressure. Reprinted, with permission, from [24], Debenedetti P G, *Metastable Liquids , Concepts and P r inciples* copyright (1996) Princeton University Press, and adapted originally from [57].

Table 2. Measurements of supercooled water's isobaric heat capacity.

Range[a]	Reference
1 bar; −7.5/31 °C	[65]
1 bar; −35(H), −30(D)/5 °C	[55]
1 bar; −38(H), −34(D)/5 °C	[66]
1 bar; −38(H), −33(D)/4 °C	[67]
1 bar; −35/17 °C	[68][b]
1 bar; −37(H), −33(D)/17 °C	[69]
1 bar; −28.5/10 °C	[70]
1 bar; −37/12 °C	[71]

[a] H = H_2O; D = D_2O. Measurements are for H_2O unless otherwise indicated.
[b] Study on $H_2O + H_2O_2$ and $H_2O + N_2H_4$. Contains also H_2O data.

moderate supercooling [65]. Calculations based on the thermodynamic identity

$$c_v = c_p - vT\frac{\alpha^2}{K_T} \tag{4}$$

and the measured density, compressibility and thermal expansion predict that c_v does not increase anomalously upon supercooling.

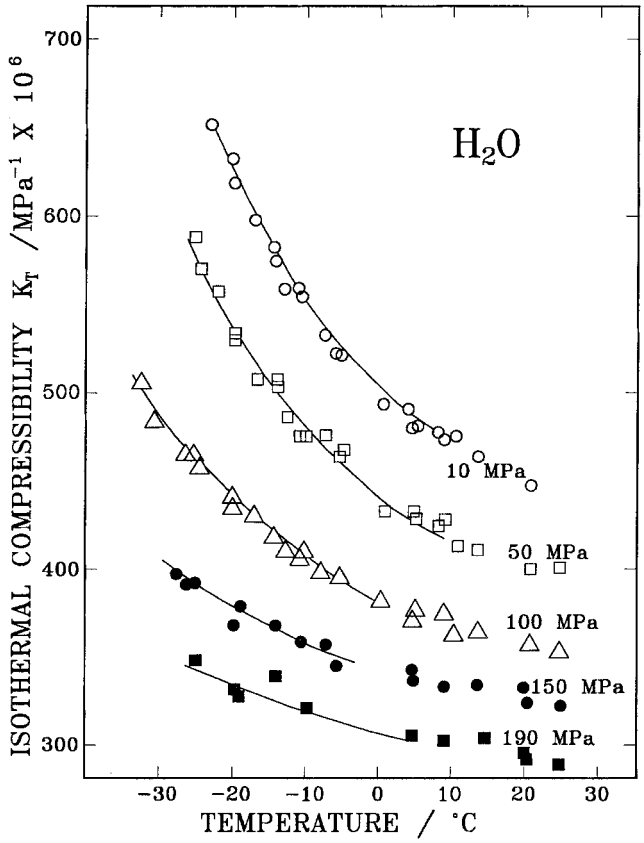

Figure 9. The temperature dependence of supercooled water's isothermal compressibility at several pressures. Lines are fits of experimental data to power-law divergences as per equation (11), with exponent $\gamma = 0.373$. Reprinted, with permission, from [24], Debenedetti P G, *Metastable Liquids, Concepts and Principles* copyright (1996) Princeton University Press, and adapted originally from [61].

5.3. Sound velocity

The hydrodynamic sound velocity is given by

$$c = (\rho_{\mathrm{m}} K_s)^{-1/2} = (\rho_{\mathrm{m}} K_T c_v / c_p)^{-1/2} \tag{5}$$

where ρ_{m} is the mass density and K_s the adiabatic compressibility: $K_s = (\partial \ln \rho / \mathrm{d}P)_s$. Trinh and Apfel [72] used the diffraction of a laser beam by an ultrasonic standing wave (about 3 MHz) to measure the sound velocity in supercooled water at atmospheric pressure down to $-16.75\,^{\circ}\mathrm{C}$. The data show a decrease from 1410 m s^{-1} at $0\,^{\circ}\mathrm{C}$ to 1310 m s^{-1} at $-16.75\,^{\circ}\mathrm{C}$. The opposite trend would apply for a normal liquid, that is to say one whose adiabatic compressibility decreases upon cooling. The same authors [73] calculated the speed of sound from thermodynamic data, using equation (5), and predicted a minimum with respect to temperature around $-25\,^{\circ}\mathrm{C}$. Using an acoustic levitation technique, Trinh and Apfel [74] measured the sound velocity down to $-33\,^{\circ}\mathrm{C}$ at 54 kHz. The data show a levelling-off of the sound velocity below $-25\,^{\circ}\mathrm{C}$, with a possible minimum around $-30\,^{\circ}\mathrm{C}$ ($c \approx 1230$ m s^{-1}), although experimental uncertainties prevent the unambiguous characterization of the low-temperature trends as levelling-off versus showing an extremum.

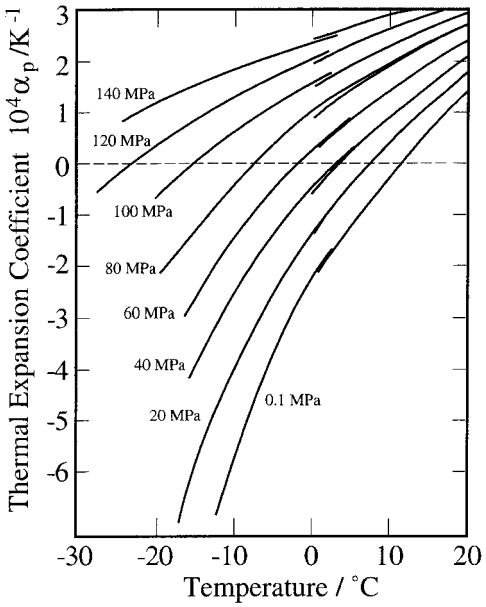

Figure 10. The temperature dependence of the thermal expansion coefficient of supercooled D_2O at several pressures. The high-temperature portions of the isobars are from [313]. Reprinted, with permission, from [24], Debenedetti P G, *Metastable Liquids, Concepts and Principles* copyright (1996) Princeton University Press, and adapted originally from [56].

Speed of sound measurements in supercooled water under pressure ($\leqslant$3.5 kbar) were performed by Petitet *et al* [75].

Rouch *et al* [76] used Brillouin scattering to study sound propagation in supercooled water down to $-9\,^{\circ}$C in the GHz range. This method involves measuring the frequency of sound waves generated by the scattering of a single-frequency laser beam,

$$c = \frac{\omega_B \lambda}{4\pi n \sin(\theta/2)} \tag{6}$$

where the measured quantity is ω_B, the Brillouin frequency ($f = \omega_B/2\pi$ is the sound wave frequency), λ is the laser beam wavelength, n is water's index of refraction and θ is the scattering angle. Results from this technique, subsequently extended to $-20\,^{\circ}$C by Teixeira and Leblond [77] and by Conde *et al* [78], show monotonically decreasing sound velocity upon supercooling, as do the measurements of Bacri and Rajaonarison [79] down to $-26\,^{\circ}$C.

To date, the discrepancy at $T \leqslant -23\,^{\circ}$C between the measurements of Apfel and co-workers [72–74], which span the kHz–MHz range and suggest the existence of a sound velocity minimum (adiabatic compressibility maximum), and the GHz-range Brillouin scattering measurements [76–79] that show a monotonic decrease in the sound velocity have not been resolved. One possible interpretation of this discrepancy is an anomalous dispersion relationship in deeply supercooled water, whereby the sound velocity would decrease with increasing frequency. Subsequent studies aimed at probing sound dispersion in supercooled water, however, have ruled out this possibility [80–82]. Using Brillouin scattering (1–10 GHz), Magazú *et al* [80] and Cunsolo and Nardone [81] observed positive dispersion and a well-defined minimum in the sound velocity with respect to temperature that shifts towards higher temperatures with increasing frequency.

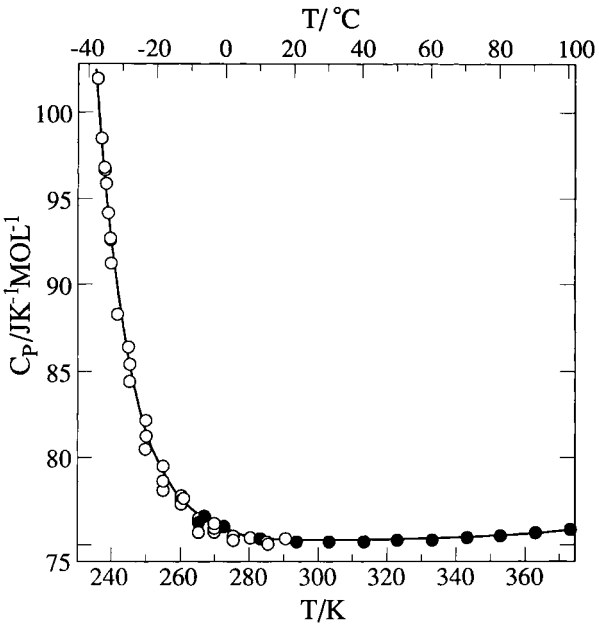

Figure 11. The temperature dependence of supercooled water's isobaric heat capacity c_p at atmospheric pressure. Literature data (●) included in the original [69], as well as measurements of Angell *et al* (○). Reprinted, with permission, from [24], Debenedetti P G, *Metastable Liquids, Concepts and Principles* copyright (1996) Princeton University Press, and adapted originally from [69].

As predicted by Rahman and Stillinger via molecular dynamics [83], water's dynamic structure factor exhibits two modes. The high-frequency mode shows linear dispersion for wavevectors q above about 4 nm^{-1}, with velocity 3200 m s^{-1}, as observed in stable D_2O by means of inelastic neutron scattering [84] and in stable [85–88] and supercooled [82, 89] H_2O by means of inelastic x-ray scattering. It was thought originally that this high-frequency mode corresponded to a second, 'fast sound', perhaps associated with hydrogen dynamics. However, the similarity of the spectra in H_2O and D_2O indicates that this mode is a centre-of-mass property. The velocity changes progressively from 3200 to 1500 m s^{-1} upon decreasing q below 4 nm^{-1} [86], indicating that water's 'fast sound' [83] is simply the normal longitudinal acoustic branch, which is subject to a positive dispersion. This interpretation is consistent with simulations [90, 91], and has been rendered quantitative through measurements of the density dependence of the sound velocity [88] and the temperature dependence of the relaxation time [89]. The low-frequency mode is weakly dispersive, and when extrapolated to $q = 0$ it implies a sound velocity of about 1500 m s^{-1}. However, simulations [92] and comparisons between water and ice [86] have shown that this mode has a large transverse component at large wavevectors, whereas sound waves are longitudinal. Ruocco and Sette [93] have reviewed this topic recently.

5.4. Miscellaneous static properties

Table 3 lists measurements of the dielectric constant, vapour pressure and surface tension of supercooled water.

Table 3. Measurements of supercooled water's dielectric constant, vapour pressure and surface tension.

Property	Range[a]	Reference
Dielectric constant	1 bar; −36/20 °C	[94]
	1 bar; −35/0 °C	[95]
	1 bar; −17/20 °C	[96]
	1 bar; −16.5/32 °C	[97]
Vapour pressure	−15/−3 °C	[98]
	−14(H), −12(D)/−2(H), 2(D) °C	[99]
	−2.5/5 °C	[100]
	−22(H), −15.5(D)/0(H), 3(D) °C	[101]
Vapour–liquid interfacial tension	1 bar; −8/−5 °C	[102]
	1 bar; −22.2/27 °C	[103]
	1 bar; −27.2/60 °C	[104]
	1 bar; −21/24 °C	[105]

[a] H = H_2O; D = D_2O. Measurements are for H_2O unless otherwise noted.

Table 4. Measurements of supercooled water's self-diffusion coefficient.

	Range[a]	Reference
Supercooled		
	1 bar; −25/30 °C	[106]
	1 bar; −31/25 °C	[107]
	1/2380 bar; −20/2 °C	[108]
	1/3000 bar; −20/0 °C	[109]
	1/4000(H), 2000(D) bar; −70(H), −30(D)/0(H), 180 °C(D)	[19]
	1/3500 bar; −21.5/0 °C	[110]
	1 bar; −35.4/25 °C	[111]
	1 bar; −29/25 °C(D)	[112]
	2000/4000 bar; −39/22 °C(D)	[113]
Glassy → supercooled[b]		
	1 bar; −123/−113 °C	[49, 114]

[a] H = H_2O; D = D_2O. Measurements are for H_2O unless otherwise indicated.
[b] Experiments involve heating an initially glassy film above its apparent glass transition.

5.5. Diffusion coefficient

Experimental measurements of supercooled water's self-diffusion coefficient are listed in table 4. They fall into two categories: results from studies performed on supercooled water and on glassy water. In the latter case, the experiments (described below) involved heating an amorphous sample and the measured diffusivities may pertain to deeply supercooled and highly viscous water.

In addition to the studies listed in table 4, mention must be made of the pioneering incoherent quasi-elastic neutron scattering investigations of diffusive motions in supercooled water by Chen *et al* [115] and Teixeira *et al* [116]. These authors studied water at atmospheric pressure and over the temperature range $-20\,^{\circ}\mathrm{C} \leqslant T \leqslant 20\,^{\circ}\mathrm{C}$. They identified two relaxation times: a short time τ_1 associated with rotational relaxation ($\tau_1 \approx 2$ ps at $-20\,^{\circ}$C) and an intermediate time τ_2 associated with translational motion of the water molecule ($\tau_2 \approx 23$ ps at $-20\,^{\circ}$C). τ_1 was found to exhibit Arrhenius behaviour, whereas the temperature dependence of τ_2 was found to be non-Arrhenius. By fitting the scattering linewidth to a jump diffusion model

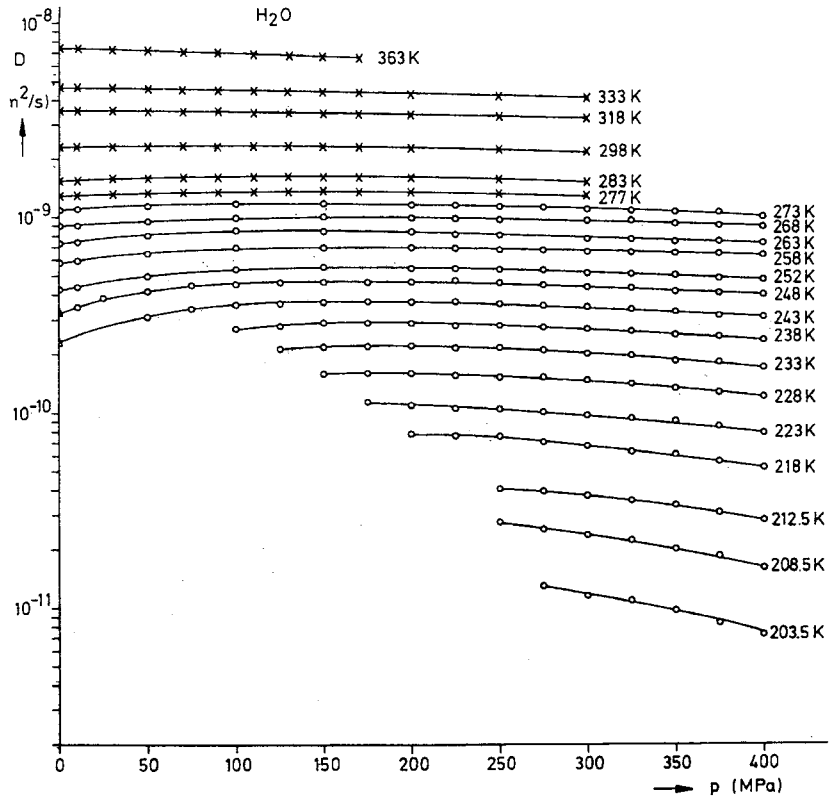

Figure 12. The pressure dependence of liquid water's self-diffusion coefficient at several temperatures. Reprinted, with permission, from [19].

these authors were also able to calculate a jump distance that increased upon supercooling (e.g., $L = 1.29$ Å at 20 °C and 2.39 Å at −20 °C). It was not possible to determine accurate values for the self-diffusion coefficient at low temperatures because under these conditions the linewidth was lower than the half-width at half-maximum of the instrument's resolution function [116].

Figure 12 shows the pressure and temperature dependence of supercooled water's self-diffusion coefficient [19]. At atmospheric pressure the diffusivity decreases almost 15-fold between 25 and −35 °C [107]. Notably, the diffusivity increases with pressure at low enough temperatures ($T \leqslant$ about 10 °C [19, 108, 109]). The isobaric temperature dependence at 1 bar shows deviations from Arrhenius behaviour, with an effective activation energy that increases at lower temperatures to about 45 kJ mol^{-1} at −31 °C [7].

In a remarkable study, Kay and co-workers measured the extent of isotope exchange and mixing in vapour-deposited thin films of amorphous water using temperature-programmed desorption [49, 114, 117, 118]. Amorphous solid water (ASW) films were formed by molecular beam deposition onto Au(111) and Ru(001) single-crystal substrates. Isotopically labelled $H_2{}^{16}O$ and $H_2{}^{18}O$ nanoscale films (<5000 Å thick) were deposited sequentially on top of each other, and temperature-programmed desorption was used to measure quantitatively the desorption kinetics and thereby reveal the extent of mixing between the films of different isotopic composition [49]. The substrates were heated by means of a resistance, from 85 K to a temperature above which the films had completely desorbed [117]. Quantification of the temperature-dependent diffusivity was done by fitting a one-dimensional transport model to the

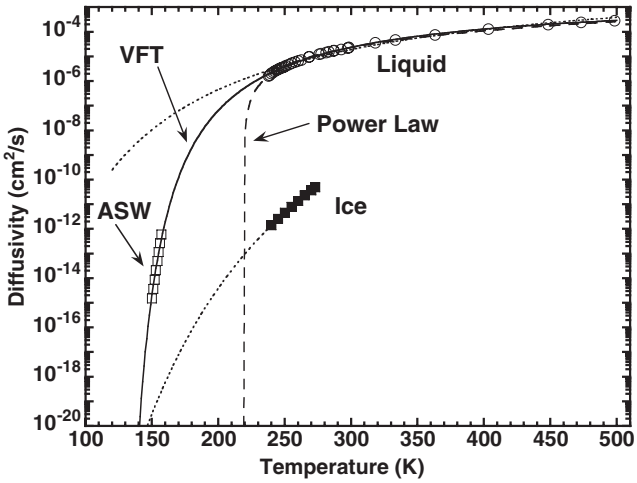

Figure 13. The temperature dependence of the diffusion coefficient in ASW films heated above the glass transition (□). Diffusion coefficients were calculated by fitting isotopic intermixing data from temperature-programmed desorption experiments [49, 114]. Also shown are diffusivity data for liquid water (○) [19, 107, 111] and ice (■) [314, 315]. The full line is a fit of the ASW data to the Vogel–Tammann–Fulcher form (see equation (8)), with singular temperature $T_0 = 119 \pm 3$ K. The dashed line is a fit of the supercooled liquid data to a power-law form such as equation (7), with singular temperature 219.2 K and exponent 1.74. Reprinted from [114], Smith R S *et al* 2000 *Chem. Phys.* **258** 291. Copyright (2000), with permission from Elsevier.

Table 5. Measurements of supercooled water's shear viscosity.

Range[a]	Reference
1 bar; −9.3/0 °C	[119]
1 bar; −24/0 °C	[120]
1 bar; −8/40 °C	[121]
1 bar; −35(H), −31(D)/0(H), 4 °C(D)	[122]
1/6000 bar; −15/10 °C	[18][b]

[a] H = H_2O; D = D_2O. Measurements are for H_2O unless otherwise indicated.
[b] Data for stable water; includes extrapolated values for supercooled water at −15 °C.

experimentally measured desorption rates [118]. The heating protocol apparently caused the glassy films to go through the glass transition in the 135–140 K range[1] and then to crystallize to cubic ice (Ic) in the 150–160 K range. The calculated diffusivities are shown in figure 13. Both the magnitude and the temperature dependence of the diffusion coefficient are consistent with the idea that highly supercooled water is formed above the glass transition and below the onset of crystallization. Comparison with ice diffusion data suggests that the film did not crystallize in the 150–157 K range. For bulk samples the onset of crystallization occurs at 150 K [28, 31], so presumably the delayed crystallization is due to interactions with the substrate.

5.6. Shear viscosity

Table 5 lists measurements of supercooled water's shear viscosity.

The shear viscosity of liquid water at atmospheric pressure increases sharply upon supercooling, and displays non-Arrhenius behaviour (figure 14). As shown in figure 4, the

[1] The assignment of water's glass transition temperature is controversial, however. See section 6.1.

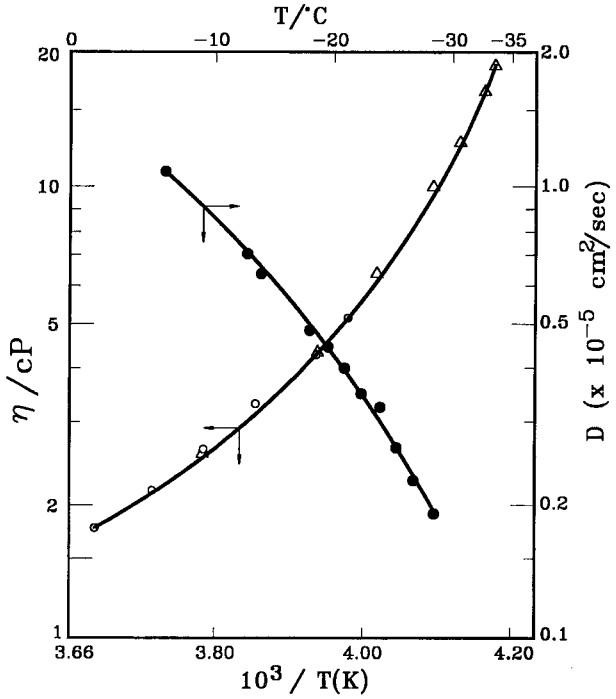

Figure 14. An Arrhenius plot of the shear viscosity of supercooled water at atmospheric pressure [122]. Diffusivity data [107] are also shown. Reprinted, with permission, from [24], Debenedetti P G, *Metastable Liquids, Concepts and Principles* copyright (1996) Princeton University Press.

viscosity of water decreases upon compression for $T \leqslant 306$ K [1, 18]. However, no actual measurements exist of the pressure dependence in the supercooled region. The data reported in [18] are for stable water, although some extrapolated values at supercooled conditions are included in the paper.

5.7. Miscellaneous dynamic properties

In an important body of work, Lüdemann and collaborators investigated relaxation processes in supercooled water over a wide range of temperatures and pressures by measuring nuclear magnetic relaxation times [113, 123–127]. The orientational correlation time τ_θ was calculated from measurements of spin–lattice relaxation in ^{1}H, ^{2}H and ^{17}O nuclei. Agreement between the results obtained by the emulsion-based technique used by Lang and Lüdemann and the analogous but bulk measurements of DeFries and Jonas [18] indicates that the behaviour of water in about 6 μm droplets [123] is indistinguishable from that observed in the bulk. Below about 1 kbar, Lang and Lüdemann found that the isobaric temperature dependence of τ_θ could be described by a power law of the form

$$\tau_\theta = \tau_0 \left(\frac{T - T_s}{T_s} \right)^{-\gamma}. \tag{7}$$

At $P \geqslant$ about 1.5 kbar, on the other hand, the data were well represented by a Vogel–Tammann–Fulcher (VTF) form

$$\tau_\theta = \tilde{\tau}_0 \exp\left(\frac{B}{T - T_0} \right). \tag{8}$$

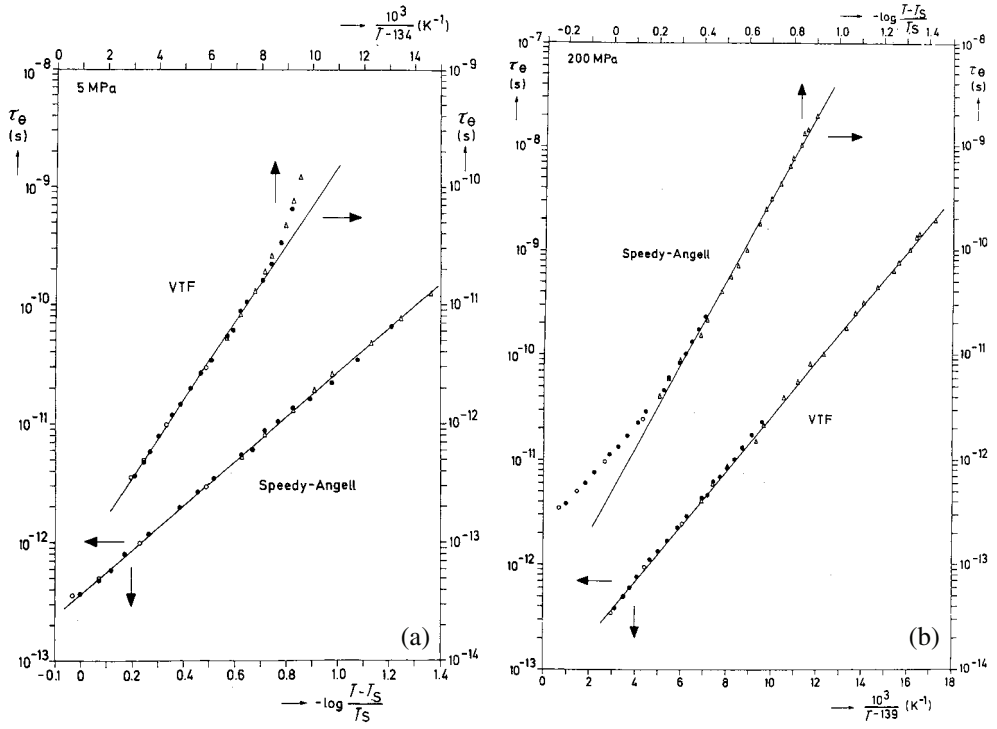

Figure 15. The temperature dependence of the orientational correlation time τ_θ for D_2O at 50 bar (left) and 2 kbar (right). Data are plotted according to equations (7) (Speedy–Angell) and (8) (VTF), with singular temperatures T_s, $T_0 = 229$, 134 K (50 bar) and 175, 139 K (2 kbar). Reprinted, with permission, from [125].

Figure 15 shows that equations (7) and (8) provide accurate representations of the experimental data over some three decades of orientational correlation time at low and high pressures, respectively. Figure 16 shows the singular temperatures obtained from these fits. This suggests a gradual transition, upon application of pressure, from dynamics dominated by proximity to an apparent singularity (equation (7); see section 7.5), to regular viscous liquid behaviour (equation (8)). Earlier studies by Hindman and collaborators investigated proton and deuterium spin–lattice relaxation in supercooled water at atmospheric pressure [128, 129].

The dielectric relaxation time of supercooled water has been measured down to −18 °C by Bertolini *et al* [97], and at modest supercoolings ($T \geqslant 270$ K), for both H_2O and D_2O, by Rønne *et al* [130–132]. Bertolini *et al* found that supercooled water could be described by a single dielectric relaxation time, showing Arrhenius temperature dependence. Rønne *et al* [130–132] fitted the frequency dependence of the complex dielectric constant to a double Debye model, and obtained fast (fs) and slow (ps) relaxation times. The temperature dependence of the slow (Debye) process was well represented by a Debye–Stokes–Einstein-type relation (according to which the quantity $T\tau/\eta$, where τ is the dielectric relaxation time and η the shear viscosity, should be constant), as well as by an expression such as equation (7), with $T_s = 228$ K (235 K for D_2O).

6. Properties of glassy water

Water, like any other liquid, can be vitrified when cooled sufficiently fast as to avoid crystallization. Unlike other substances, however, water can apparently form at least two

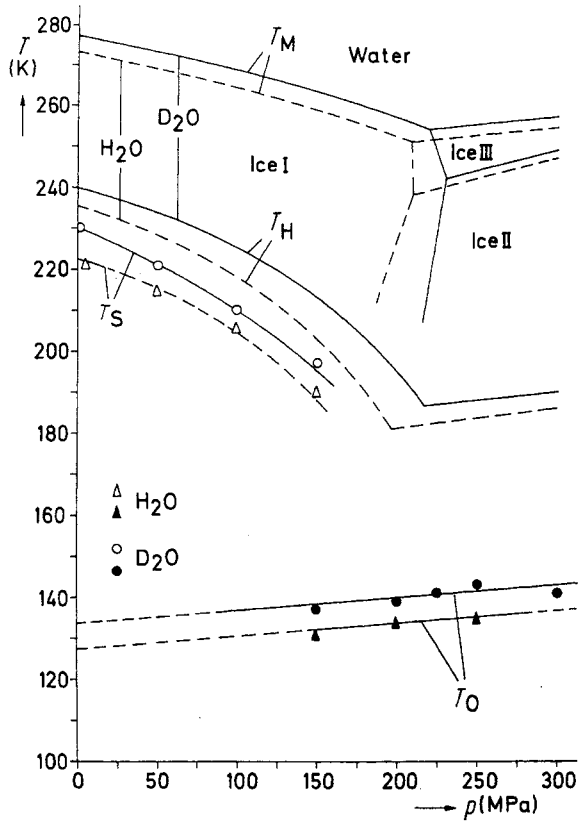

Figure 16. The pressure and isotope dependence of the singular temperatures T_s (equation (7) and figure 15) and T_0 (equation (8) and figure 15) for water's orientational correlation time τ_θ. Also shown are the melting T_M and homogeneous nucleation (T_H) temperatures. Reprinted, with permission, from [125].

distinct forms of glass. Of these, two have been extensively studied: they are known as low-density and high-density amorphous ice (LDA and HDA, respectively). The properties of LDA and HDA, and the nature of the transition between them, are key to understanding the thermodynamics of supercooled and stable liquid water. Recently, very-high-density amorphous ice (VHDA) has been proposed as a third distinct form of glassy water [3].

6.1. Low-density amorphous ice (LDA)

The first laboratory report on the formation of ASW by rapid cooling dates back to 1935, when Burton and Oliver [133] found that an amorphous solid was formed when water vapour at low pressure was deposited on a sufficiently cold substrate. A large body of experimental work has since confirmed this observation (e.g., [134, 135]). Typically, thin films of vapour-deposited ASW are grown on single-crystal substrates (e.g., Au(111), Ru(001), Pt(111)) at deposition rates between 0.1 and 7 μm h^{-1} and temperatures between 10 and 120 K, using molecular beams [118, 136]. The morphology and physical properties of ASW films depend sensitively on the growth angle, thermal history of the film and substrate characteristics [137–141].

The direct vitrification of liquid water was first achieved by Brüggeller and Mayer [142] by ejecting a pressurized emulsion of μm-size water droplets in *n*-heptane onto liquid ethane

Table 6. Irreversible transformations between water's non-crystalline forms.

Step[a]	Conditions	Reference
1	Vapour deposition on cold substrate (e.g., 77 K)	e.g., [135]
2	Anneal in vacuo at 113 K	e.g., [29]
3	Hyperquench μm-sized droplets on cryoplate	e.g., [146]
4	Anneal at 130 K	[28]
5	Quench emulsified water below 130 K at 10^4 K s^{-1} at about 5 kbar	[154]
6	Compress ice Ih at 77 K to about 10 kbar	e.g., [149]
7	Decompress HDA at 77 K, then heat to about 120 K at 1 bar	e.g., [149, 150]
8	Compress LDA at 77 K to about 5 kbar	e.g., [150]
9	Isobaric heating of HDA to 165 K at 11 kbar	[155]
10	Isobaric heating of HDA to 177 K at 19 kbar	[155]
11	Isochoric heating of VHDA from 77 to about 140 K starting at 200 bar	[155]
12	Isobaric heating of VHDA from 77 to about 127 K at 1.1 kbar	[155]

[a] See figure 18.

at 90 K. These authors subsequently vitrified pure (non-emulsified) water by projecting a high-speed thin jet into liquid propane at 80 K [143]. Variants of this method have important applications in electron microscopy [144, 145]. Using rapid cooling of small aerosolized water droplets (3 μm $\leqslant d \leqslant$ 25 μm) onto a metal cryoplate (15 K $\leqslant T \leqslant$ 77 K), Mayer was able to vitrify liquid water without resorting to a liquid cryomedium [146]. Vitrification of water by rapid cooling of the liquid is referred to as hyperquenching, since it requires cooling rates of about 10^6 K s^{-1}; the resulting material is called hyperquenched glassy water (HGW).

After annealing in vacuum from 77 to about 113 K [29], ASW relaxes to a material that is indistinguishable from HGW. This identity has been confirmed by calorimetry [20], x-ray and neutron scattering [147], and Raman spectroscopy [148]. Another route to glassy water is to compress hexagonal ice at 77 K to about 11 kbar, decompressing the resulting material and heating it to about 120 K [149, 150]. The high-density phase obtained by compressing ordinary ice is called HDA, and is discussed in detail in sections 6.2 and 6.3. The material produced by decompressing HDA and heating is called LDA. X-ray and neutron diffraction measurements suggest that LDA is structurally identical to HGW and annealed ASW [147] (figure 17). Because of small differences between the apparent glass transition temperatures of LDA and HGW, as well as subtle structural differences revealed by incoherent inelastic neutron scattering [151, 152], it has been suggested that HGW and LDA are different materials [153]. It seems more likely, however, that such residual differences reflect variations in the method of preparation and experimental procedures, such as annealing [22]. The consensus view at present is that LDA, HGW and annealed ASW are the same material [3, 22]. The irreversible transformations between water's various non-crystalline forms are illustrated in figure 18 and table 6. Table 7 lists measurements of important thermophysical properties of LDA.

As mentioned in section 4, when LDA is heated to about 150 K, it crystallizes to ice Ic (cubic ice) [31]. Thus, in the range of temperatures from 136 to 150 K, non-crystalline water would appear to be a highly viscous liquid slightly above its glass transition. Using a blunted conical indenter, Johari [50] showed that LDA does indeed deform under load and behaves like a viscous liquid near 143 K. Jenniskens *et al* [51] also reported liquid-like behaviour in thin ASW films in the range 140–210 K. The isotope exchange experiments of Kay and co-workers (see [49, 114, 117, 118]; figure 13) are also consistent with the notion of ultraviscous liquid water in the vicinity of 150 K. On the other hand, Fisher and Devlin [161] investigated isotope exchange reactions in ASW and concluded that the data were inconsistent with the occurrence

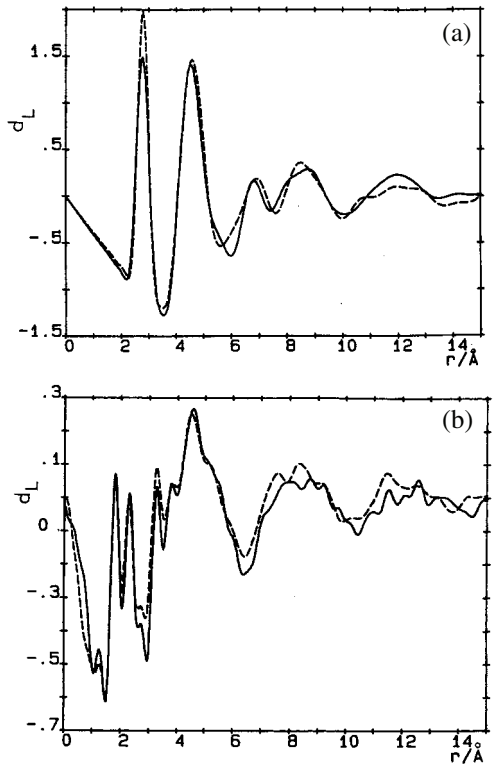

Figure 17. (a) The weighted molecular pair correlation function, $d_L = 4\pi r\rho[g(r) - 1]$ of HGW at 77 K (solid curve) and LDA (dotted curve), determined by means of x-ray diffraction. Here r is the intermolecular separation and $g(r)$ is the centre-of-mass radial distribution function. (b) The weighted intermolecular pair correlation function of HGW at 77 K (solid curve) and LDA (dotted curve), determined by means of neutron diffraction. The intermolecular function is obtained by Fourier transforming the difference between the static structure factor and the molecular form factor, yielding only the contribution from intermolecular terms. Note the structural similarity between HGW and LDA. Reprinted, with permission, from [147].

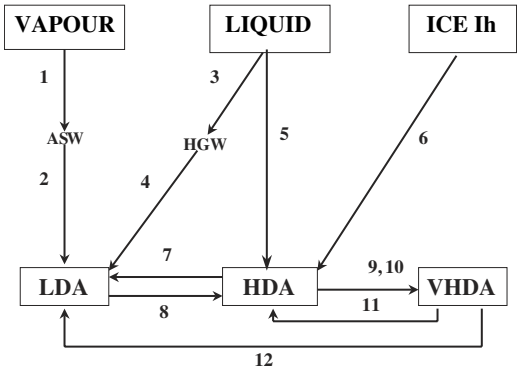

Figure 18. Irreversible transformations between water's various non-crystalline forms. See table 6 for details on the paths.

of translational diffusion. They suggested instead that the molecular motion that develops as ASW is heated through its glass transition is rotational.

Table 7. Measurements of thermophysical properties of LDA.

Property	Conditions[a]	Reference
Density (g cm^{-3})		
0.94 ± 0.02	ASW, 82/110 K, 1 bar	[156]
0.94	ASW, 77 K, 1 bar	[135]
0.94 ± 0.02	LDA[b], 117 K, 1 bar	[150]
Heat capacity[c] (J mol^{-1} K^{-1})		
14.94	LDA[b,d], 90 K, 1 bar	[157][e]
19.78	LDA[b,d], 124 K, 1 bar	[157][e]
Glass transition (K)		
136 ± 1	HGW, 1 bar, 30 K min^{-1}[f]	[28]
136 ± 1	HGW, 1 bar, 30 K min^{-1}[f]	[158]
136	ASW[g], 1 bar, 30 K min^{-1}[f]	[29]
124	LDA[b,h], 1 bar, 10 K h^{-1}[f]	[157]
129 ± 2	LDA[b], 1 bar, 30 K min^{-1}[f]	[153]
137	HGW(D), 1 bar, 30 K min^{-1}[f]	[159]
Heat capacity[c] change at T_g (J mol^{-1} K^{-1})		
1.9 ± 0.2	ASW[g], 1 bar, 136 K	[29]
1.6 ± 0.1	HGW, 1 bar, 136 K	[158]
1.8 ± 0.2	HGW(D) 1 bar, 137 K	[159]
Enthalpy of crystallization to ice Ic (kJ mol^{-1})		
-1.66 ± 0.27	LDA[b], 1 bar, 152 K	[149]
-1.33 ± 0.02	HGW, 1 bar, 159–163 K	[31]
-1.29 ± 0.01	ASW[g], 1 bar, 150 K	[29]
-1.43 ± 0.03	HGW, 1 bar, 150 K	[159]
-1.44 ± 0.08	HGW(D), 1 bar, 156 K	[159]
Entropy with respect to ice Ih (J mol^{-1} K^{-1})		
1.7 ± 1.7	ASW[i], 1 bar, 150 K	[160]

[a] $D = D_2O$. Results are for H_2O unless otherwise indicated.
[b] LDA obtained by heating of decompressed (1 bar) HDA.
[c] Isobaric.
[d] Average over three LDA samples, annealed at 124, 129 and 130 K for 2 h.
[e] [157] gives tabular data in the 90–136 K range.
[f] Heating rate in differential scanning calorimetry.
[g] ASW deposited at 77 K and annealed in vacuum up to about 113 K.
[h] Annealed in the 124–130 K range.
[i] Thin film deposited from a molecular beam. Entropy calculated from the evaporation rate.

Recently, Angell and co-workers have argued that the glass transition of water should be reassigned to 165 ± 5 K [8, 30]. They noted that the excess enthalpy of HGW is still unrelaxed at 150 K when crystallization to ice Ic begins. Studies of hyperquenched liquids show that the excess enthalpy associated with being trapped in a high-energy configuration upon very rapid cooling is completely relaxed at 1.1 T_g [8] Thus, for water, and using the commonly accepted value of 136 K for T_g (see table 7), the frozen-in excess enthalpy should relax completely at 149 K, in contrast to what actually occurs. If, however, the glass transition temperature is revised to $\sim$165 K, water's enthalpy recovery exotherm exhibits behaviour similar to that of other hyperquenched glass formers [8]. The proposed reassignment is controversial, as is the interpretation of calorimetric data on which it is based [162, 163]. The implication is that water's true glass transition temperature at atmospheric pressure would not be observable, since it would occur above the temperature of spontaneous crystallization to ice Ic. This does not explain water's apparently liquid-like behaviour at 142 K [50]. On the other hand, it provides

Table 8. Measured values of the density of HDA.

Density (g cm^{-3})	Conditions	Reference
1.31	77 K, 10 kbar[a]	[149]
1.17	77 K, 1 bar[b]	[149]
1.26 ± 0.02	77 K, 6 kbar[c]	[150]
1.19 ± 0.02	77 K, 1 bar[d]	[150]

[a] HDA produced by compression of ice Ih.
[b] HDA produced by compression of ice Ih and then decompressed to 1 bar.
[c] HDA produced by compression of LDA.
[d] HDA produced by compression of LDA and then decompressed to 1 bar.

a plausible explanation for the notion that two different forms of water (water A, formed upon heating ASW or HGW; and water B, formed upon heating LDA) do not interconvert even when heated above the 'conventional' T_g [153], as well as for the failure of amorphous water films to exhibit the isotopic scrambling expected for liquid-like behaviour [161]. At present, the precise assignment of water's glass transition temperature is a subject of debate. Most experimental observations are consistent with the 'conventional' value, $T_g \sim 136$ K.

6.2. High-density amorphous ice (HDA)

As first shown by Mishima and co-workers in 1984, application of pressure to ice Ih at low temperature leads to the formation of an amorphous solid, which has come to be known as high-density amorphous ice (HDA) [149]. The idea behind the original experiment was to cross the metastable extrapolation of hexagonal ice's melting curve. Because this locus has negative slope in the (P, T) plane, it (or its metastable extrapolation) will be crossed upon compression of the stable solid phase. By choosing a temperature, 77 K, low enough to thwart kinetically the transformation into stable ice IX, and also such that any liquid phase would be below its glass transition, Mishima and co-workers succeeded in amorphizing ice Ih through a process that started at 10 kbar and was completed by 15 kbar.

Upon decompression to atmospheric pressure, HDA at 77 K remains a dense solid (1.17 g cm^{-3} [150]; compare with table 7), which transforms irreversibly to LDA upon heating to about 120 K [150]. Upon compressing LDA at 77 K, Mishima and co-workers observed an abrupt transition to HDA, accompanied by a 22% volume decrease, at 6 kbar [150][2]. Measured values of the density of HDA are given in table 8.

The nature of the transformation from ice Ih to HDA remains incompletely understood. Initially interpreted as a first-order melting transition of a crystal into a glass [149], it has been the subject of experimental [32] and computational investigation [152, 164, 165]. It has been argued that above 165 K the first-order melting mechanism applies, but below 140 K the compression of ice Ih leads to a mechanical instability in the crystal lattice [152, 165]. A recent neutron diffraction study of the structure of HDA, however, found no evidence of microcrystallinity, thus calling into question the mechanical instability argument, and strongly suggesting that ice Ih indeed melts into HDA [166].

Compression of HDA at 77 K leads, at 40 kbar, to a crystalline phase similar to orientationally disordered ice VII [167]. At higher temperatures, about 150 K, HDA transforms to a crystalline phase similar to ice VIII around 20 kbar [167]. The structure of HDA decompressed to ambient pressure has been studied by means of x-ray diffraction [168] and neutron scattering [151, 166, 169, 170]. Figure 19 shows a comparison of the short-range

[2] The apparently reversible transition between LDA and HDA is discussed in section 6.3.

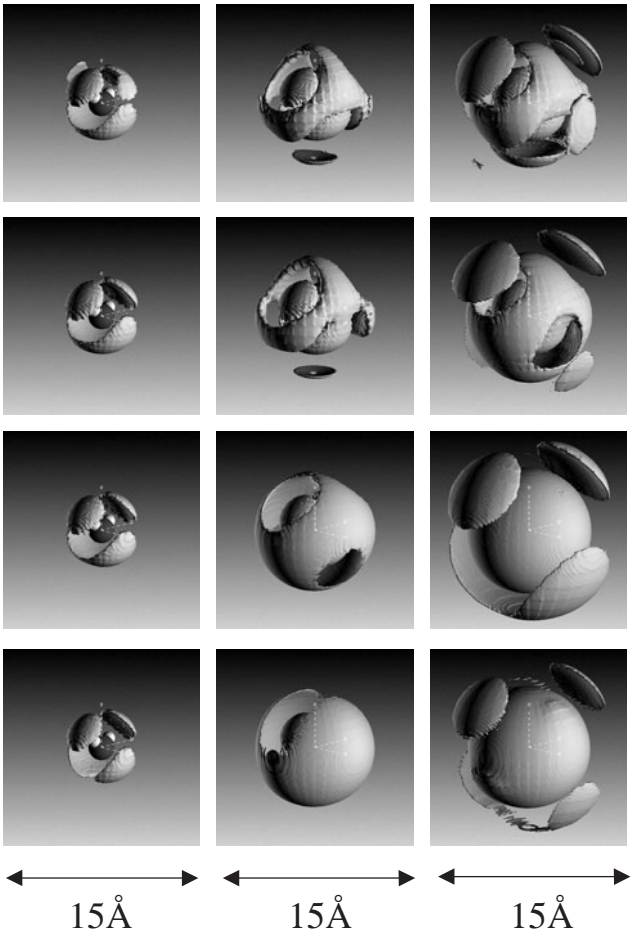

Figure 19. Contours of constant density around a central water molecule showing the distribution of (left to right) the first-, second- and third-neighbour water molecules for (top to bottom) HDA at 80 K, liquid water at 298 K, LDA at 80 K and ice Ih at 220 K. The contour levels are for intermolecular radial distribution function values of (2.1, 1.5, 1.2; left to right; top), (1.7, 1.3, 1.1), (2.3, 1.7, 1.2), (3.1, 2.1, 1.5; bottom). The contours were calculated by Monte Carlo simulation to generate ensembles of water molecules whose structure is consistent with the measured diffraction data. Reprinted, with permission, from [166] Finney J L *et al* 2002 *Phys. Rev. Lett.* **88** 225503. Copyright (2002) by the American Physical Society.

structures of HDA, LDA, ice Ih and liquid water in the form of spatial density functions [166]. It can be seen that there are significant local order similarities between LDA and ice Ih, and between HDA and liquid water. The similarity between liquid water and HDA extends to the second and third coordination shells, supporting Mishima's view [149] that there is a first-order melting transition to HDA upon compression of cold ice Ih [166]. The study of Finney *et al* [166] includes the first experimental determination of the three site–site distribution functions (H–H, O–O, O–H) of LDA and HDA. Klotz *et al* [171] studied the structure of HDA under pressure, up to about 22 kbar.

Recently Mishima and Suzuki apparently succeeded in forming HDA by rapid cooling (10^3–10^4 K s^{-1}) of emulsified liquid water under pressure (about 5 kbar; see figure 18 and table 6) [154]. The material formed below 130 K, when examined by Raman spectroscopy and

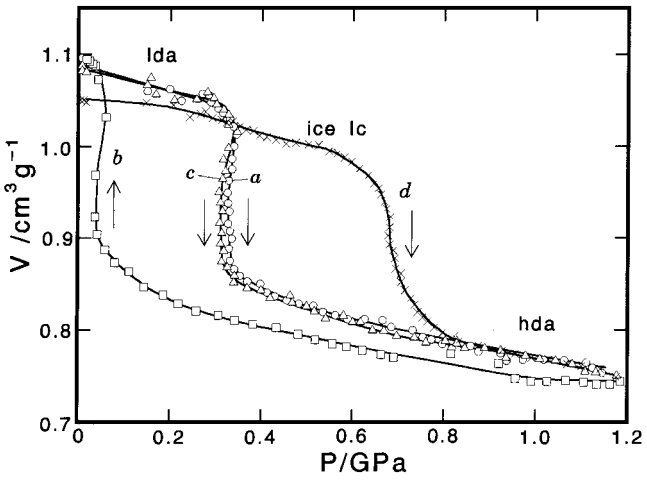

Figure 20. The reversible transition between LDA and HDA. The data show the evolution of the volume as a function of applied pressure during compression (a), subsequent decompression (b) and recompression (c) of amorphous phases during warming from 130 to 140 K. Compression of ice Ic at ∼145 K is also shown (d). Reprinted, with permission, from [172].

using x-ray diffraction at atmospheric pressure and 77 K, yielded a spectrum similar to that of decompressed HDA. Furthermore, upon heating at 1 bar an abrupt transformation to a low-density phase was observed at 130 K (entirely analogous to the decompressed HDA-to-LDA transition), and this low-density material in turn yielded a Raman spectrum similar to that of LDA. The glass transition of the material (presumably HDA) formed by cooling emulsified water under pressure has not yet been measured.

6.3. The transition between LDA and HDA

In 1985 Mishima and co-workers compressed LDA (formed by heating decompressed HDA at atmospheric pressure above 130 K, and then rapidly cooling to 77 K) and observed a sharp transition at 6 ± 0.5 kbar [150]. The transition entailed an about 22% volume decrease, and did not reverse when the pressure was decreased. By increasing the temperature to about 135 K, Mishima showed that the transition can be reversed [172] (figure 20). Table 9 lists thermodynamic quantities associated with the apparently first-order transition between LDA and HDA.

The sharpness and reversibility of the transformation are consistent with a first-order transition between LDA and HDA. The equilibrium pressure P_{eq} for a first-order transition satisfies the thermodynamic identity

$$P_{\mathrm{eq}} = -\frac{\Delta u}{\Delta v} + T_{\mathrm{eq}}\frac{\mathrm{d}P}{\mathrm{d}T} \tag{9}$$

where T_{eq} is the equilibrium temperature, Δu and Δv are the differences in internal energy and volume between the coexisting phases, and $\mathrm{d}P/\mathrm{d}T$ is the slope of the equilibrium transition line in the (P, T) plane. Using the low-pressure value of the enthalpy difference between LDA and HDA for Δu, and the measured volume difference (see table 9), the calculated equilibrium pressure is at most 1.9 kbar [175, 176]. Since the transition from HDA to LDA is exothermic, the second term on the right-hand side of equation (9) is negative, and allowing for this quantity would make the calculated equilibrium pressure less than 1.9 kbar. Thus, the

Table 9. Measurements of thermodynamic properties associated with the apparently first-order transition between LDA and HDA.

Property	Conditions	Reference
Transition pressure (kbar)[a]		
6 ± 0.5	77 K	[150, 172]
2	135 K	[172]
Volume change ($cm^3\ g^{-1}$)[b]		
−0.22	77 K	[150]
−0.2	135 K	[172]
Enthalpy change ($J\ mol^{-1}$)[c]		
530[d]	114 K, 1 bar	[173]
756 ± 144	117 K, 1 bar	[149]
507 ± 54[e]	107–130 K, 1 bar	[174]

[a] The value of the pressure at which the transition is observed. Includes the non-equilibrium overpressurization.
[b] v(HDA) − v(LDA).
[c] h(HDA) − h(LDA).
[d] Does not include the 244 J mol^{-1} due to annealing HDA between 85 and 105 K.
[e] Does not include the enthalpy of annealing of HDA.

measured transition pressure is close to equilibrium at 135 K, but a sizable overpressure must be applied at 77 K to overcome kinetic sluggishness.

The progress of the LDA–HDA transition has been followed visually [177, 178], as well as by Raman spectroscopy [178] and using neutron diffraction [179]. The observation of a well-defined propagating phase boundary [178] supports the notion of a first-order phase transition. In contrast, a recent neutron and x-ray diffraction investigation of structural changes in recovered (atmospheric pressure) HDA upon annealing has been interpreted as implying that the transition to LDA proceeds through a series of metastable intermediates [180] (see also section 7.4). However, the temperatures in that study (95, 100, 105 and 110 K) were all below 135 K, the thermal level required for the transition to be reversible (see figure 20) and hence the observations are instead fully consistent with incomplete structural relaxation upon annealing. The elastic properties of LDA and HDA in the transition region have been investigated ultrasonically. Both heating of recovered HDA and compression of LDA lead to softening of the shear modulus [181, 182].

6.4. Very-high-density amorphous ice (VHDA)

Recently Loerting *et al* [155] reported that an apparently distinct form of high-density amorphous ice can be recovered at 77 K and atmospheric pressure, following isobaric heating of HDA under pressure. They called this material very-high-density amorphous ice (VHDA). Specifically, they heated HDA at 11 kbar from 77 K up to 165 K, and at 19 kbar from 77 K to 177 K (see figure 18). The resulting material relaxed at atmospheric pressure and 77 K to the same structure, as characterized by x-ray diffraction and Raman spectroscopy, and had a density of 1.25 g cm^{-3}, that is to say ∼9 % higher than recovered HDA. Upon isochoric heating from 77 K to 140 K starting from a pressure of 2 kbar, VHDA was found to convert back to HDA. Isobaric heating at 1.1 kbar to 127 K yielded LDA, with no intermediate formation of HDA. Both the Raman spectrum and the x-ray diffraction pattern of VHDA differ from those of HDA.

The detailed structure of VHDA has been determined by Finney *et al* via neutron diffraction with isotope substitution [183], with site–site radial distribution functions and spatial density

distributions calculated by the empirical potential structure refinement Monte Carlo procedure. The OH and HH radial distribution functions of recovered VHDA were found to be very similar to those of HDA, but significant differences were found in the respective OO distributions. The first OH coordination number for VHDA is 2, indicating that each water molecule participates in two hydrogen bonds, and hence that VHDA is a fully coordinated hydrogen bond network. Integration of the area under the OO first peak out to the first minimum in HDA reveals that the number of nearest neighbours increases from 5 in HDA to 6 in VHDA [183]. These differences notwithstanding, Klotz *et al* [171] noted that the structure of recovered VHDA is very similar to that of HDA at about 7 kbar.

Loerting *et al* [155] found that the volume decreased continuously during isobaric heating of HDA. However, the recovered samples at 77 K and 1 bar showed just one distinct structure. They interpreted this observation as implying that pressurized amorphous ice with a continuum of densities relaxes upon depressurization to a new form of amorphous water, VHDA. Whether this recovered state is indeed a new form of amorphous water, or just a kinetically trapped structure, is not known at present.

7. Interpretations

7.1. Stability limit conjecture

In 1982 Speedy [184] proposed an interpretation of the thermodynamics of metastable water, according to which the increase in response functions upon supercooling is caused by the approach to the spinodal curve where superheated liquid water becomes unstable with respect to the vapour phase. A schematic representation of the stability limit conjecture is shown in figure 21. Its salient feature is the continuous spinodal curve bounding the superheated and supercooled regions. In normal liquids, the liquid spinodal has a positive slope in the (P, T) plane, and the zero-temperature limit of the spinodal curve yields the upper bound for the liquid's tensile strength (e.g., 27 times the critical pressure for the van der Waals fluid [24]). In water, according to Speedy's conjecture, the spinodal would instead retrace towards positive pressures, and would therefore be approached upon isobaric supercooling. Because the spinodal is a locus of diverging density and entropy fluctuations [24], retracing would indeed explain the experimentally observed increase in water's compressibility and heat capacity.

Thermodynamic consistency demands that the slope, in the (P, T) plane, of a spinodal curve must change sign upon encountering a line along which the thermal expansion coefficient vanishes [184–186]. This is shown in figure 21, where at 'e' the liquid attains its maximum tensile strength and its spinodal curve retraces its path after encountering the TMD line[3] 'fae', along which $\alpha = 0$. Between curves 'fae' and 'fe', the liquid's thermal expansion coefficient is negative. This is shown by isochores 'g' and 'h' ($\rho_g > \rho_h$). The former becomes tangent to the spinodal with negative slope (pressure increase upon isochoric cooling); the latter with positive slope. The change in slope of the spinodal follows from the fact that it is an envelope of isochores [24, 185]; that is to say, at the spinodal the following equation is satisfied:

$$\left(\frac{\mathrm{d}P}{\mathrm{d}T}\right)_{\mathrm{sp}} = \left(\frac{\partial P}{\partial T}\right)_{\rho}. \tag{10}$$

The left-hand side denotes the slope of the spinodal in the (P, T) plane, and the right-hand side, the slope of an isochore, evaluated at the spinodal. In addition to the tangency condition

[3] See also section 3.

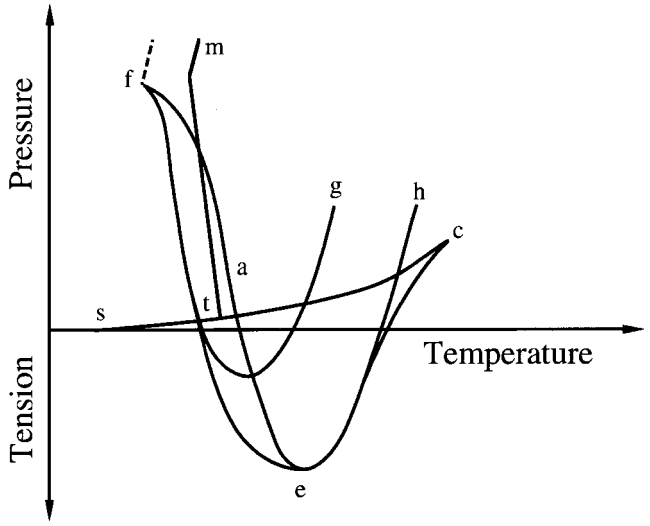

Figure 21. A schematic representation of Speedy's stability limit conjecture. 'st' is the sublimation curve, 'tc' is the boiling curve and 'tm' is the melting curve. 'g' and 'h' are isochores ($\rho_g > \rho_h$), 'c' and 't' are the critical and triple points, respectively. 'fae' is the locus of density maxima and 'cef' is the continuous spinodal bounding the superheated, supercooled and simultaneously superheated–supercooled states. Reprinted, with permission, from [24], Debenedetti P G, *Metastable Liquids, Concepts and Principles* copyright (1996) Princeton University Press.

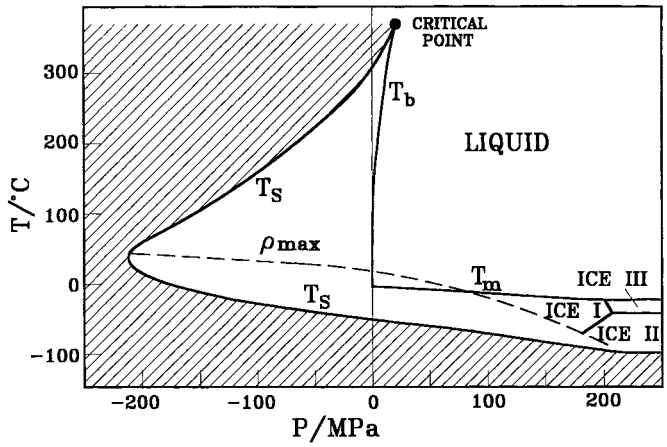

Figure 22. The phase diagram of water, showing the postulated continuous, retracing spinodal according to Speedy's stability limit conjecture. Reprinted, with permission, from [24], Debenedetti P G, *Metastable Liquids, Concepts and Principles* copyright (1996) Princeton University Press, and adapted originally from [316].

given by equation (10), the slope of isochores must satisfy the requirement that it vanish along 'fae'. If, starting anywhere along 'fe', the temperature is increased isobarically, the density will increase, reach a maximum along 'fae' and decrease thereafter: line 'fae' is a locus of density maxima. Thus, according to the stability limit conjecture, water's TMD locus causes its liquid spinodal to retrace its path to positive pressures, providing a continuous boundary for superheated, stretched and supercooled states. This scenario is illustrated in figure 22.

A hitherto unnoticed implication of the stability limit conjecture all but rules out its validity as a plausible interpretation of water's thermodynamics. Two non-conjugate thermodynamic variables (e.g., temperature and pressure; temperature and density) specify the equilibrium state of a pure substance. A retracing spinodal such as 'ef' must intersect the metastable continuation of the vapour–liquid equilibrium curve (not shown in figures 21 or 22). Any point in the (P, T) plane along a phase coexistence locus corresponds to two different densities (e.g., saturated liquid and vapour along 'tc'). The spinodal 'cef' is a locus of liquid state points. Therefore, the intersection of the retracing branch 'ef' with the metastable boiling curve must correspond to the same liquid state. This can only be possible if the spinodal and the binodal coincide, which implies that the intersection of the retracing spinodal and the metastable boiling curve is a critical point. Therefore, if the superheated liquid spinodal retraces its path to positive pressures, the vapour–liquid coexistence locus must have both upper and lower critical points. The former is the normal vapour–liquid critical point. Although a metastable lower critical point for water's vapour–liquid transition cannot be ruled out, there is no experimental evidence that such a point exists.

The implausible lower critical point for the vapour–liquid transition would only occur if a spinodal curve were to retrace to positive pressure. Several microscopic models of water-like fluids show a retracing spinodal curve that does not extend to positive pressure. In lattice models with directional interactions due to Sastry *et al* [187], Sasai [188] and Borick *et al* [189], the intersection of the TMD and the liquid spinodal causes the latter to retrace. However, the spinodal does not reach positive pressure, and is superseded by a locus of limits of stability of the supercooled liquid with respect to the solid phase. A lattice model with spherically symmetric nearest-neighbour attraction and next-nearest-neighbour repulsion also exhibits spinodal retracing, but the spinodal curve reaches a low-temperature limiting value $P = 0$ at $T = 0$ [190].

Within the framework of the stability limit conjecture, data for deeply supercooled water are often fitted to the form

$$X = X_0 + A\left(\frac{T}{T_s} - 1\right)^{-\gamma} \tag{11}$$

where X is a thermodynamic quantity that diverges at the spinodal, A is a constant, T_s is the singular (spinodal) temperature and X_0 is the background, non-diverging component. Under the assumption that the Helmholtz energy is an analytic function of temperature and density at the spinodal, $\gamma = 1/2$ should be observed upon isobaric cooling [24, 191]. Data analysis according to equation (11) yields ambiguous results [24, 57]. This follows not just from the implausibility of a spinodal singularity upon supercooling, but also from the experimental limitations imposed by homogeneous nucleation on the possibility of approaching the conjectured singularity close enough to make power-law fits reliable [24]. For example, at the homogeneous nucleation temperature of 231 K, the quantity $(T/T_s - 1)$ equals 0.01 for $T_s = 228$ K [60], compared to 10^{-3} or better for state-of-the-art critical-phenomena experiments (see, e.g., [192]). Although the stability limit conjecture is a strictly thermodynamic theory, the notion of a supercooled liquid spinodal has also been used in the analysis and correlation of transport and relaxation properties (e.g., [60]). Equation (7) and figure 15 illustrate this approach, which is discussed further in section 7.5.

The stability limit conjecture played an important role in the search for a coherent picture of metastable water's overall behaviour. An incisive and useful exercise in thermodynamic consistency, its implausibility is, however, rendered evident by the same type of macroscopic, model-independent reasoning invoked in its formulation. That it has taken more than twenty years to uncover this flaw highlights the subtlety of the arguments involved.

7.2. Second critical point

The second-critical-point interpretation was formulated in 1992 by Poole *et al* [193]. It links the anomalies of supercooled water to the transition between LDA and HDA. In so doing it provides a thermodynamically consistent perspective on the global phase behaviour of metastable water, and has opened up a rich new area of research in liquid-state physics that has come to be known as polyamorphism (e.g., [194, 195]). According to this view, the transition between the two forms of amorphous water is first order and terminates at a critical point. The experimentally observed increases in liquid water's heat capacity, compressibility and magnitude of the thermal expansion coefficient upon cooling are the macroscopic manifestation of the increased density and entropy fluctuations (see equations (3)) associated with this critical point, above which the two metastable forms of amorphous water become indistinguishable [193]. The experimentally observed transition between LDA and HDA is interpreted as the structurally arrested manifestation of an equilibrium phase transition between two forms of liquid water: low-density liquid (LDL) and high-density liquid (HDL), of which LDA and HDA are simply the corresponding vitreous forms [196–198]. The novelty of these ideas and the elegant simplicity of the resulting picture remain as striking today as when this interpretation was put forward more than a decade ago.

When water freezes to ice Ih it expands. In supercooled water, transient domains where molecules adopt arrangements with high tetrahedral symmetry form spontaneously by thermal fluctuations [20, 21]. It is energetically favourable for these low-density domains to share edges and faces without the introduction of strain [14]. Consequently their average size increases upon cooling. The potential therefore exists for a transition between a denser, disordered phase and a less dense but more structured phase. In the second-critical-point scenario this transition involves actual discontinuities of volume and entropy: it is a first-order phase transition. Because the high-density phase is also the one with the largest entropy, the phase transition locus has a negative slope in the (P, T) plane, and the critical point associated with this transition corresponds to the temperature above which (and, unusually, the pressure *below* which) the difference between the coexisting phases vanishes (figure 23).

The second-critical-point interpretation was formulated as a result of extensive molecular dynamics simulations of the ST2 model of water [199]. Poole *et al* [193] observed that low-temperature isotherms of this model exhibit an inflection point at high pressure; the shape and temperature dependence of the inflection region are similar to what would be observed if a critical point were approached. Non-equilibrium isothermal compression of low-temperature, low-density amorphous solid ST2 in fact yielded sharp inflections at which the volume changed abruptly, suggesting the existence of a first-order phase transition between two amorphous solid forms of ST2. The inflections of the supercooled liquid isotherms and the isothermal compression simulations of the low-density amorphous solid are shown in figure 24. The response functions of ST2 water increase in the supercooled region in qualitative agreement with experimental observations. Similar behaviour was found [200] for the TIP4P model of water [201]. Poole *et al* also investigated the behaviour of the liquid spinodal and its relationship to the TMD. Under sufficiently high tensions (negative pressure), the TMD was found to retrace towards lower temperatures and did not intersect the spinodal. Hence their calculated spinodal displayed a monotonic positive slope in the (P, T) plane and did not retrace towards positive pressure. This is illustrated in figure 25.

Molecular simulations of LDA and HDA include detailed comparisons with the structure determined by means of neutron scattering and an analysis of stability limits that is consistent with the existence of a first-order transition between LDA and HDA [202].

Strong if not definitive experimental support for the second-critical-point interpretation was obtained by Mishima and Stanley [203]. In a very clever set of experiments, these authors

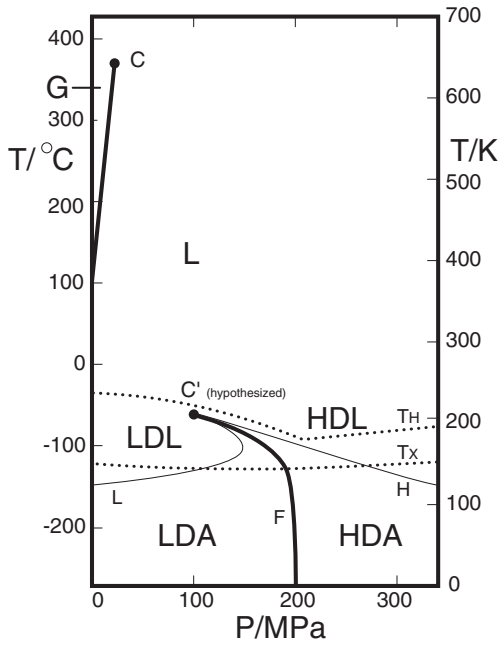

Figure 23. The phase diagram of the non-crystalline forms of water showing the second-critical-point interpretation. C and C′ are the vapour–liquid and liquid–liquid critical points, respectively. F is the coexistence line along which low- and high-density liquid phases (LDL, HDL) coexist. At low enough temperatures, the liquid phases become structurally arrested into their corresponding vitreous forms (LDA, HDA). Lines L and H are the limits of stability (spinodal curves) for HDL and LDL, respectively. T_H is the homogeneous ice nucleation locus and T_X denotes the temperature of spontaneous crystallization (to ice Ic at low pressure). Reprinted, with permission, from [22]. Copyright (1998) *Nature*. (http://www.nature.com/).

measured the melting curve of metastable ice IV. They observed that this locus undergoes a sharp change of slope in the region where it would intersect the presumed line of first-order liquid–liquid phase transitions. Results from similar experiments on D_2O ices are shown in figure 26 [204]. Since none of these solid phases undergoes abrupt changes along its melting line, the sudden change in slope must be due to a corresponding change in the nature of the liquid phase into which the solid melts. This follows from the Clausius–Clapeyron equation

$$\frac{\mathrm{d}P}{\mathrm{d}T} = \frac{\Delta s}{\Delta v} \tag{12}$$

where $\mathrm{d}P/\mathrm{d}T$ denotes the slope of the melting curve in the (P, T) plane, and Δs and Δv denote the difference in molar entropy and volume, respectively, between the coexisting liquid and solid phases. The experiments were performed by decompressing an emulsion of deionized water droplets (40% by volume; droplet size 1–10 μm) in a continuous methylcyclopentane–methylcyclohexane phase with sorbitan tristearate surfactant. Starting from the region of stability of the ice phase, that is to say high pressure and low temperature, an about 1 cm^3 sample of the emulsion contained in an indium capsule was decompressed isothermally until melting occurred, causing the temperature to decrease. The partially melted and endothermically cooled sample was then decompressed again, causing further melting (the sample was not maintained at fixed temperature). This is how the melting curves shown in figure 26 were measured.

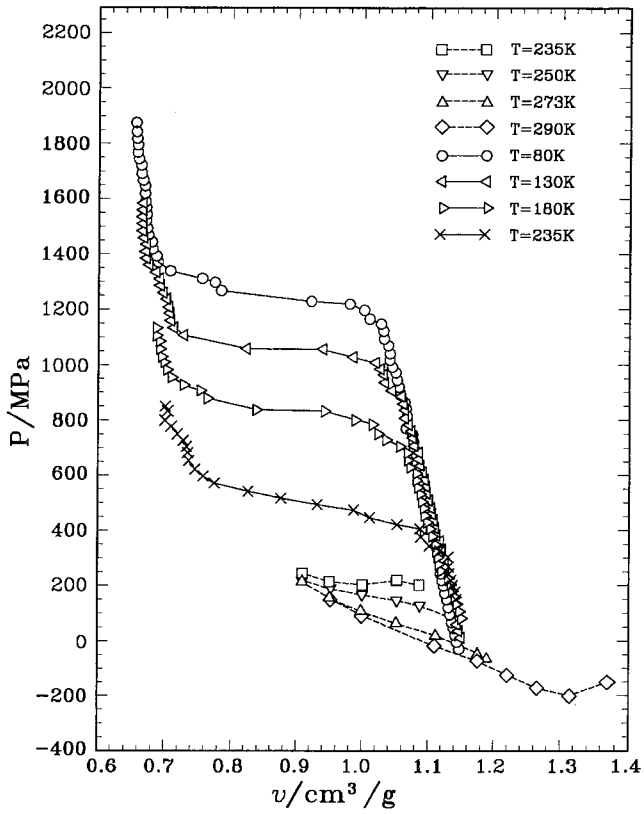

Figure 24. Isothermal compression curves for LDA obtained by molecular dynamics simulation of ST2 water (full lines), and low-temperature portions of liquid isotherms showing inflection points (dashed lines). Note the abrupt decrease in volume upon compression into an apparently different amorphous phase. The compression curves were generated by increasing the pressure by 25 MPa every 10 ps. The solid curves are non-equilibrium processes, as can be seen by comparing the liquid and solid curves at 235 K. Reprinted, with permission, from [24], Debenedetti P G, *Metastable Liquids , Concepts and Principles* copyright (1996) Princeton University Press, and adapted originally from [193].

Mishima and Stanley constructed the Gibbs free energy surface for supercooled water on the basis of the equality of liquid and crystal chemical potentials along any melting curve. They further assumed that the difference in volumes between high-pressure forms of ice and ice Ih is constant over the temperature and pressure ranges 77–300 K and 0–1.5 kbar, and that the corresponding entropy difference is negligible. Differentiation of the Gibbs surface yields the equation of state, which predicts a low-temperature critical point at approximately 1 kbar and 220 K [203].

Two factors render these elegant experiments not fully conclusive. First, the alternative thermodynamic interpretation of supercooled water's thermodynamics, namely the singularity-free scenario discussed in section 7.3, also posits sharp, albeit continuous, changes in entropy and volume. The practical impossibility of distinguishing sharp from discontinuous changes in the slope of a melting line renders the experimentally determined curves less-than-definitive proofs of the existence of a first-order liquid–liquid transition. Secondly, the hypothesized line of first-order transitions appears to track the homogeneous nucleation locus quite closely (see

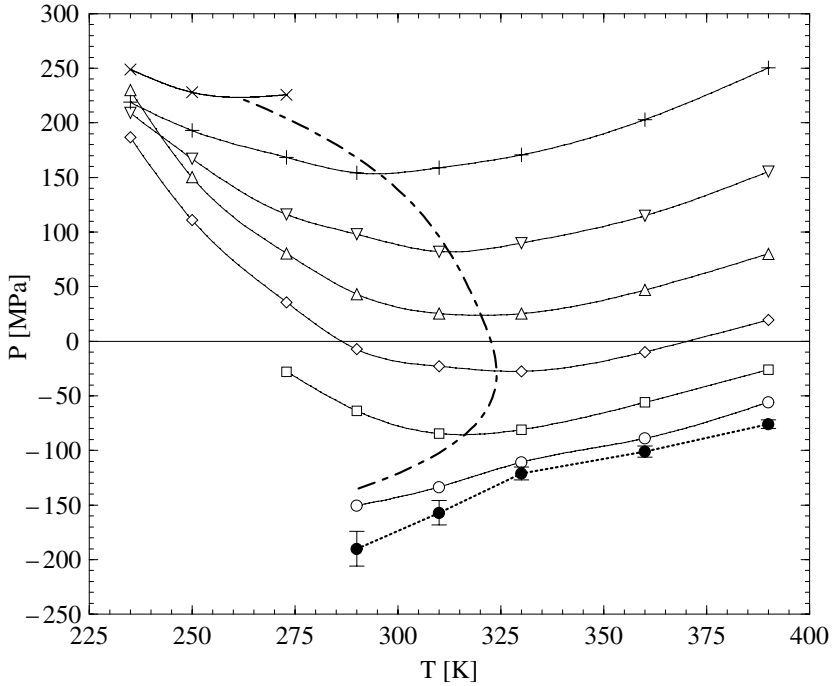

Figure 25. Isochores (full lines), TMD locus (- — -) and liquid spinodal (....) for ST2 water. The densities are 1.1 (×), 1.05 (+), 1 (▽), 0.95 (△), 0.9 (◇), 0.85 (□) and 0.8 (○) g cm^{-3}. The TMD line is the locus of minima along isochores and the spinodal line is the locus of minima along isotherms. Note the retracing TMD and consequently the monotonic spinodal. Reprinted, with permission, from [200] Poole P H *et al* 1993 *Phys. Rev.* E **48** 3799. Copyright (1993) by the American Physical Society.

figure 23). Thus, the change in slope of the melting curve may also reflect the sudden freezing of the partially melted liquid. These caveats notwithstanding, the work of Mishima and Stanley represents the best evidence to date in support of the second-critical-point interpretation of supercooled water's thermodynamics. Note that the change in slope of the melting curves shown in figure 26 becomes less abrupt as the temperature at which such a change occurs becomes higher and the pressure becomes lower. This too is consistent both with the second-critical-point and the singularity-free (section 7.3) scenarios.

Molecular simulation of several water and water-like models has shown direct evidence of low-temperature liquid–liquid immiscibility. Roberts *et al* [205] used Monte Carlo simulation of a lattice model [206] with strong directional bonding, and found a phase transition between two liquid phases with upper and lower critical points, in agreement with theoretical predictions [206]. Using molecular dynamics simulation of the ST2 potential with a reaction field treatment of Coulombic interactions, Harrington *et al* [207] constructed pressure versus density isotherms and found that an inflection developed upon lowering the temperature. In particular, at the lowest temperature examined, $T = 235$ K, a 15% change in density did not cause the pressure to increase. The second critical point for the ST2 potential was estimated to occur at approximately 235 K and 2 kbar [207, 208]. Evidence of liquid–liquid phase separation at low temperatures in ST2 water has also been obtained by imposing a strong gravitational field and calculating the resulting density profile [209]. Pressure–density isotherms of the TIP5P model of water [210] also show evidence of a low-temperature transition between

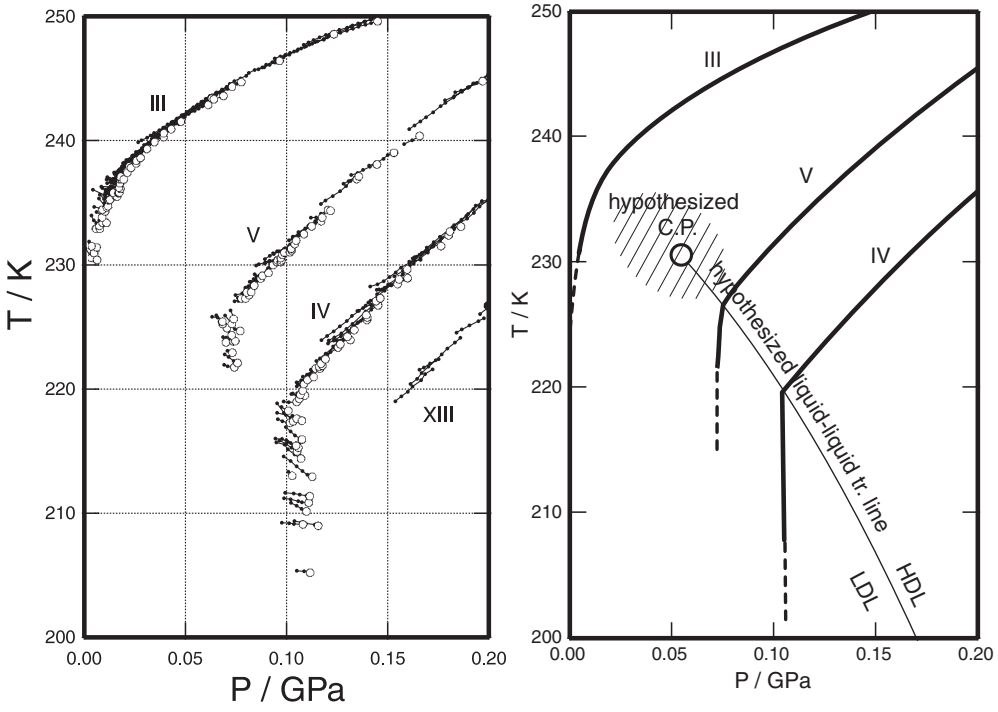

Figure 26. Melting curves of D_2O ices (III, V, IV, XIII). Left: experimental results, with circles indicating the onset of the change in sample temperature during the decompression-induced melting experiment. Right: a schematic representation of the hypothesized liquid–liquid transition between high- and low-density liquids (HDL, LDL). CP denotes the hypothesized critical point. Reprinted, with permission, from [204] Mishima O 2000 *Phys. Rev. Lett.* **85** 334. Copyright (2000) by the American Physical Society.

two liquid phases, with an estimated critical point occurring at 217 ± 3 K, 3.4 ± 0.2 kbar and 1.13 ± 0.04 g cm^{-3} [211]. In all of these studies, substantial numerical uncertainties associated with finite-size effects prevent accurate location of the critical point. Nevertheless, evidence of a liquid–liquid transition can be considered conclusive in the case of the ST2 and TIP5P potentials.

Brovchenko *et al* [212] reported three liquid–liquid transitions in ST2 water at low temperatures. Their method involved restricting density fluctuations (see., e.g., [213, 214]) so that the simulated system remains homogeneous in the coexistence region. The ST2 potential was treated with a simple spherical cut-off and no long-range electrostatic correction. An interesting observation in this study is the fact that the critical point for the first liquid–liquid transition (i.e., the one with the highest critical temperature and lowest critical density) occurs at negative pressure. This is in contrast to the calculations of Harrington *et al* [207], and points to the importance of studying systematically the effects of long-range electrostatics, as well as of the imposition of constraints on density fluctuations, on phase equilibrium predictions in molecular simulations.

In addition to the direct investigation of phase coexistence in [205, 207, 209, 211, 212], liquid–liquid immiscibility in water models has also been inferred by extrapolation [208], and by fitting the simulated free energy surface [215] to a theoretically based functional form for the internal energy. In the first case, Sciortino *et al* [208] estimated the location of the second critical point of ST2 water by extrapolation of the locus of isothermal compressibility extrema.

Scala *et al* [215] fitted the simulated values of the internal energy of the SPC/E model of water [216] to a functional form proposed by Rosenfeld and Tarazona [217] and obtained the free energy by thermodynamic integration. A liquid–liquid transition was predicted, with a critical point at 130 ± 5 K, 2.9 ± 0.3 kbar, 1.1 ± 0.03 g cm^{-3}. Tanaka [218, 219] performed molecular dynamics simulations of the TIP4P potential [201] and interpreted his results as implying the existence of a second critical point, which he estimated to occur at about 213 K and a negative pressure estimated variously to occur between 0 and -2 kbar [218], and to be not lower than -50 or -200 bar [219]. Tanaka's interpretation as to the location of a second critical point differs from that of other studies with the same or similar potentials [200, 208].

A substantial body of theoretical work has been performed, aimed at investigating the possible microscopic basis of a liquid–liquid phase transition in water from a statistical mechanical perspective. Seminal insights resulted from the modified van der Waals model of Poole *et al* [220]. In this simple and elegant theory, hydrogen bonds are partitioned into two categories: weak, for which the energy is zero, and strong, for which the energy is $-\varepsilon_{\mathrm{HB}}$. A weak bond can exist in $\Omega \gg 1$ configurations, whereas a strong bond can only exist in one configuration. These configurations differ by virtue of the mutual orientation of the two molecules participating in bond formation. Strong hydrogen bonds are most likely to occur when the bulk density has a value such that every molecule has the optimal local volume required to bond strongly to its neighbours. Away from this optimal density, a fraction f of the bonds are strong, while the remaining fraction, $(1-f)$, are weak. The density dependence of f is assumed to be a Gaussian centred at the optimal bulk density. The resulting hydrogen bond contribution to the Helmholtz energy, A_{HB}, reads ($\beta = 1/kT$)

$$-\beta A_{\mathrm{HB}} = f \ln[\Omega + \exp(-\beta\varepsilon_{\mathrm{HB}})] + (1-f)\ln(\Omega + 1) \tag{13}$$

with

$$f = \exp\{-[(v - v_{\mathrm{HB}})/\sigma]^2\} \tag{14}$$

where v is the molar volume, v_{HB} is the optimal molar volume for hydrogen bonding and σ characterizes the width of the volume interval around v_{HB} where strong bonds are favoured. The total Helmholtz energy is the sum of the usual van der Waals term plus twice the hydrogen bond contribution, equation (13), since there are two moles of hydrogen bonds per mole of molecules [220]. For an appropriate choice of parameters, the resulting equation of state displays, in addition to the customary vapour–liquid equilibrium, a low-temperature transition between two liquid phases of different density. This is shown in figure 27. For sufficiently small values of the hydrogen bonding energy, the model predicts a triple point between the vapour and the two liquid phases, and a retracing spinodal, a phase behaviour that combines aspects of the two-critical-point and stability limit pictures.

Equation (14) is an *a priori* assumption on the dependence of hydrogen bond formation on bulk density. Truskett *et al* [221] refined this approximation by solving a microscopic model of orientation-dependent bond formation. In this model, two molecules form a hydrogen bond if they exhibit mutually favourable orientations, and if one of the two participating molecules (the so-called central molecule) has a cavity of radius $r_i \geqslant d$, empty of molecular centres, surrounding it, where d is the hard-core diameter. Furthermore, the participating pair must be separated by a distance r that lies within the hydrogen bonding shell of the central molecule, with $r_i \leqslant r \leqslant r_0$. Finally, the presence of additional molecules within the hydrogen bonding shell weakens the existing bond. These geometric criteria for hydrogen bond formation introduce a positive and microscopic correlation between entropy and density, since hydrogen bond formation is favoured by a low-density local environment. Solution of

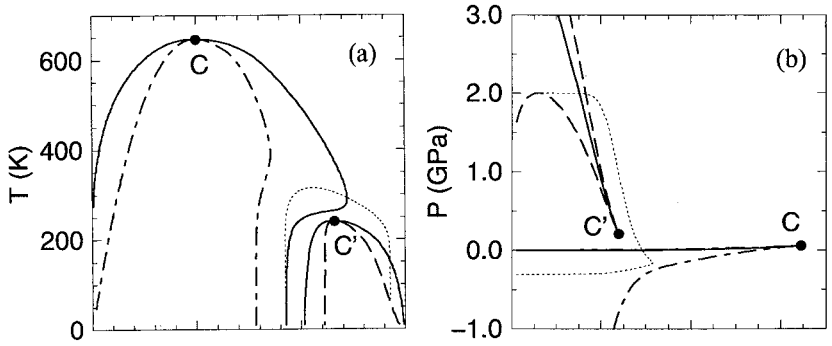

Figure 27. The phase diagram generated with the extended van der Waals model of Poole *et al* [220] in the (T, ρ) (a) and (P, T) (b) planes. $0 \leqslant \rho \leqslant 1.5$ g cm^{-3}, $0 \leqslant T \leqslant 700$ K. C and C′ are the vapour–liquid and liquid–liquid critical points, respectively. The full lines are coexistence curves, and the corresponding spinodals are shown as dashed and dot–dashed curves. The thin dotted line is the TMD locus. The parameters used in the calculation (see equations (12) and (13)) are $v_{\mathrm{HB}} = 1.087$ cm^3 g^{-1}, $\sigma = v_{\mathrm{HB}}/4$, $\Omega = 5.02 \times 10^4$, $\varepsilon_{\mathrm{HB}} = -22$ kJ mol^{-1}. Reprinted, with permission, from [220] Poole P H *et al* 1994 *Phys. Rev. Lett.* **73** 1632. Copyright (1994) by the American Physical Society.

this model in the mean-field approximation yields an equation of state of the form

$$P = P_{\mathrm{VDW}} - \rho^2 kT \sum_{i=1}^{i_{\mathrm{mx}}} \left(\frac{\partial p_i}{\partial \rho} \right)_T \ln f_i \tag{15}$$

$$f_i = \left[1 + \frac{\mathrm{i}}{4} (1 - \cos \phi^*)^2 (\exp(\beta \varepsilon_i) - 1) \right]. \tag{16}$$

In the above equations P_{VDW} is the pressure of the van der Waals fluid at the given density and temperature, and i_{mx} is the maximum number of molecules that can be present in the central molecule's hydrogen bonding shell before the strength of an existing hydrogen bond vanishes (in their calculations, Truskett *et al* considered a linear dependence of the hydrogen bond strength upon i). p_i represents the probability that, in a hard-sphere fluid at the density of interest, a given hard sphere has a cavity of radius d surrounding it and that i other spheres lie within its hydrogen bonding shell, ϕ^* is the critical angle for hydrogen bond formation, and ε_i is the energy of a hydrogen bond, weakened by the presence of the other $(i - 1)$ molecules in the central molecule's hydrogen bonding shell. The model captures many of the distinctive features of water's thermodynamics, such as density maxima, compressibility and heat capacity minima, and sharp increases in the response functions at low temperatures. It also predicts a liquid–liquid transition at low temperatures. This phase transition is very sensitive to the geometric details of the hydrogen bond, and it (though not the distinctive liquid-phase anomalies, such as negative thermal expansion) disappears upon varying ϕ^* by small amounts. Thus, the model is able to reproduce the two thermodynamically consistent scenarios for supercooled water: the second-critical-point and the singularity-free scenarios, of which the latter is discussed in section 7.3.

A third closely related analytical model of water that shows two fluid–fluid transitions and two critical points is due to Jeffrey and Austin [222]. These authors replaced equation (14) with an empirical function of temperature and density, of which the former is a low-pass filter centred at 273.15 K, and the latter is a modified Gaussian centred around an optimum density. The equation of state contains numerous adjustable parameters that somewhat limit its usefulness as a fundamental theory, although they greatly increase the accuracy of the equation for engineering calculations.

Another important theoretical contribution to the microscopic understanding of the thermodynamics of supercooled and glassy water is the recent work of Franzese and Stanley [223]. These authors considered a lattice model with directional attractions in addition to conventional nearest-neighbour interactions. These were modelled by associating with each molecule four bonding arms, and requiring that a pair of bonding arms belonging to nearest-neighbour molecules be properly oriented with respect to each other in order for a hydrogen bond to form. Since each bonding arm can adopt many orientations, only one of which leads to bonding, this introduces a strong entropic cost to bond formation. In order to account for the increase in local volume associated with hydrogen bond formation, the total volume was expressed as a sum over all lattice sites, plus an additional contribution from each bonded pair. If the four bonding arms on each molecule are modelled as independent (that is to say, the orientation of one bonding arm does not influence that of the other arms on the same molecule), this model is the one considered by Sastry *et al* [16], to be discussed in section 7.3 in connection with the singularity-free scenario. If, more realistically, intramolecular correlations between bonding arms are not neglected, the model yields two first-order phase transitions. In the low-temperature transition, the phase with higher density also has higher entropy, and hence the transition line has negative slope in the (P, T) plane.

Truskett and Dill [224, 225] introduced a two-dimensional water-like model in which each disc possesses three bonding arms arranged at 120°. The authors considered triplets of discs and distinguished between three types of fluid configuration: cage-like, dense and expanded. The former two correspond to the transient structured and unstructured regions observed in molecular simulations of water [21], and the third represents vapour states. Combining these ideas with the introduction of low- and high-density ice phases, the model of Truskett and Dill provides an appealing microscopic theory for the global phase behaviour of water. It predicts liquid-phase anomalies (density maxima, compressibility and heat capacity minima) and expansion upon freezing. It also predicts a metastable, low-temperature liquid–liquid transition with a negative slope in the (P, T) plane, terminating at a critical point.

Water-like anomalies can also arise in systems interacting via spherically symmetric potentials with two characteristic distances. The shorter distance is associated with the repulsive core, and the longer distance represents a softer repulsion that can be overcome at high enough pressure [226]. The core-softened family of potentials incorporates this feature by introducing a repulsive shoulder (for example, as a finite but constant barrier, or as a linear decrease in repulsive energy with distance). Such potentials were first used by Stell and co-workers [227–232], and have since been applied to the investigation of water-like liquid-phase anomalies [190, 233–241], including negative thermal expansion [190, 233, 236, 239], compressibility maxima [233, 239] and expansion upon freezing [233, 236, 239]. Low-temperature liquid–liquid phase transitions have also been found [190, 233–235, 237, 239, 241] including, significantly, the possibility of a negatively sloped line of liquid–liquid transitions in the (P, T) plane [239]. Liquid–liquid transitions in core-softened models, however, are generally positively sloped in the (P, T) plane [190, 233–235, 241]. This, coupled with the fact that such transitions can occur in the absence of density anomalies [226, 234], suggests that this class of models may be more appropriate to liquid metals (e.g., [242, 243]) than to water. In particular, although core-softened models illustrate well the fact that complex fluid-phase behaviour and multiple fluid–fluid transitions can result from the existence of two characteristic length scales, their spherical symmetry is too simplistic a representation to permit all but qualitative studies of global phase behaviour to apply to water.

A liquid–liquid phase transition with negative slope in the (P, T) plane, terminating at a critical point, has also been obtained in lattice models [189, 206] and in two-state models [244–247]. The interesting work of Hajime Tanaka has also provided valuable

microscopic insight [248–252]. In this approach, water's anomalies and the possibility of a second critical point are rationalized in terms of the competition between two types of local order: density and bond ordering. The former tends to minimize nearest-neighbour separation, whereas bond ordering favours the formation of open local regions with tetrahedral symmetry. These ideas have been presented both as a Landau–Ginzburg formalism [248, 249] and as a phenomenological two-state representation [250–252]. Molecular simulation of local order in realistic water models has confirmed the presence of open and comparatively structured, and dense and comparatively unstructured environments (e.g., [21, 253–256]), and related these to the liquid–liquid transition [254–256] as well as to structural, transport and thermodynamic anomalies [21].

The eleven-year period following the publication of the two-critical-point hypothesis was especially fruitful as regards theoretical and computational studies on this topic. Not only has low-temperature liquid–liquid separation been demonstrated in simulations of water-like fluids, but also a plausible microscopic basis for its occurrence has been established through the gain in entropy upon compression brought about by the disruption of low-density, tetrahedrally coordinated configurations.

7.3. Singularity-free scenario

In the singularity-free interpretation, the experimentally observed increases in water's response functions upon supercooling are explained as the thermodynamically inevitable consequences of the existence of density anomalies [16, 257, 258]. The relevant thermodynamic relations are [15, 16, 258]

$$\left(\frac{\partial K_T}{\partial T}\right)_{P,\text{at TMD}} = \frac{v^{-1}(\partial^2 v/\partial T^2)_{P,\text{at TMD}}}{(\mathrm{d}P/\mathrm{d}T)_{\text{TMD}}} \tag{1}$$

$$\left(\frac{\partial K_T}{\partial T}\right)_P = -\left(\frac{\partial \alpha}{\partial P}\right)_T \tag{2}$$

$$\left(\frac{\partial c_p}{\partial P}\right)_T = -T\left(\frac{\partial^2 v}{\partial T^2}\right)_P. \tag{17}$$

As explained in section 3, TMD denotes the locus of maximum density in the (P, T) plane—that is to say, the line defined by the condition $\alpha = 0$; and the subscripts 'TMD' and 'P, at TMD' denote a directional derivative along the TMD and a derivative evaluated at constant pressure at the TMD, respectively. Since $(\partial^2 v/\partial T^2)_P$ is positive at the TMD, and for water at positive pressure $(\mathrm{d}P/\mathrm{d}T)_{\text{TMD}}$ is negative (see figure 2), the above equations necessarily imply that, starting from any point along the TMD:

- The isothermal compressibility of liquid water increases upon isobaric cooling.
- The thermal expansion coefficient increases upon isothermal compression and becomes negative upon isothermal decompression.
- The isobaric heat capacity decreases upon isothermal compression.

Equation (2) further implies that the locus of extrema of K_T with respect to temperature along isobars coincides with the locus of extrema of α with respect to pressure along isotherms [258].

It is therefore the existence of density anomalies, in the form of a negatively sloped TMD locus, that gives rise to the experimentally observed increases in response functions. In the singularity-free scenario the response functions remain finite [62], and no underlying singularity is invoked [258]. To illustrate this possibility, Sastry *et al* [16] introduced a lattice model with nearest-neighbour attraction and directional attractions. This model has

already been described in section 7.2. Its thermal and volumetric properties were further investigated by Rebelo *et al* [258] and by La Nave *et al* [259]. If the four bonding arms on each molecule are taken to be independent (that is to say, the orientation of one bonding arm does not influence that of the other arms on the same molecule), the mean-field solution of the model yields the behaviour illustrated in figure 28. At fixed temperature, pressure suppresses anomalous behaviour; at fixed pressure, cooling gives rise to a pronounced increase in the response functions. This is illustrated in the figure by the thermal expansion coefficient, but analogous behaviour occurs for the compressibility and the heat capacity. Crucially, the increase in response functions remains finite. The higher the pressure, the lower the temperature where the pronounced increase in response function occurs, and the sharper is the increase. Since a peak in the thermal expansion coefficient indicates a sudden increase in the rate of change of volume with respect to temperature at constant pressure, the model predicts sharp increases in specific volume upon cooling, the abruptness of which increases with pressure, as shown in figure 28(b). Similarly, the corresponding increase in heat capacity gives rise to a sudden decrease of entropy upon cooling, the abruptness of which also increases with pressure [258].

An insightful early microscopic model due originally to Stanley [20, 260, 261] is in fact the earliest example of the singularity-free scenario for supercooled water. The emphasis in that work was on the behaviour of the specific model, not on the model-independent thermodynamic considerations discussed above, which have come to be associated with the singularity-free interpretation. Each water molecule i is assigned to one of j species based on the number of bonds that it can form. A bond is formed when the interaction between two molecules is stronger than an arbitrary cut-off. When implemented on a lattice, the model views each occupied site as an oxygen atom, and each bond as a hydrogen bond between neighbouring pairs of oxygen atoms. In any given configuration, molecule i can form 0, 1, 2, 3 or 4 bonds ($j = 5$) on a lattice with coordination number 4. For a given probability that two neighbour molecules are bonded, the overall concentration of molecules belonging to one of the j species is determined by random statistics; the species' connectivity, on the other hand, is highly non-random. For example, on a lattice with coordination number 4 an empty site cannot be nearest neighbour to a species-4 molecule; similarly, if the four nearest neighbours of a given site belong to species 4, then the site must also belong to species 4 [260]. In particular, the positions of tetrahedrally coordinated (species-4) oxygen atoms are strongly correlated. If the volume per site depends on the number of bonds emanating from that site, with $V_4 > V_3 > V_2 > V_1 > V_0$, then an 'ice-like' patch consisting predominantly of spatially correlated, fully bonded, species-4 molecules will have a lower local density than, say, a patch containing the same number of non-bonded molecules [253]. The spatial correlation among molecules of a given species introduces corresponding spatial correlations in density fluctuations. Consequently, as the temperature decreases, the characteristic size of the 'ice-like' patches increases and so do density fluctuations. Using these simple and insightful ideas, Stanley and Teixeira [20] made a number of qualitative predictions that agree with experimental observations. These include the increase in compressibility, isobaric heat capacity and specific volume upon cooling. The model predicts that the compressibility reaches a maximum at low temperature and remains finite upon further cooling.

Mention must also be made of the field theoretic model of water's hydrogen bond network by Sasai [262]. It includes elements of all three thermodynamic scenarios. It predicts a retracing liquid–gas spinodal; however, at low temperatures the spinodal is superseded by a locus of liquid stability limits with respect to ice-like fluctuations. Although there is no low-temperature liquid–liquid transition, the response functions diverge along the liquid–ice spinodal.

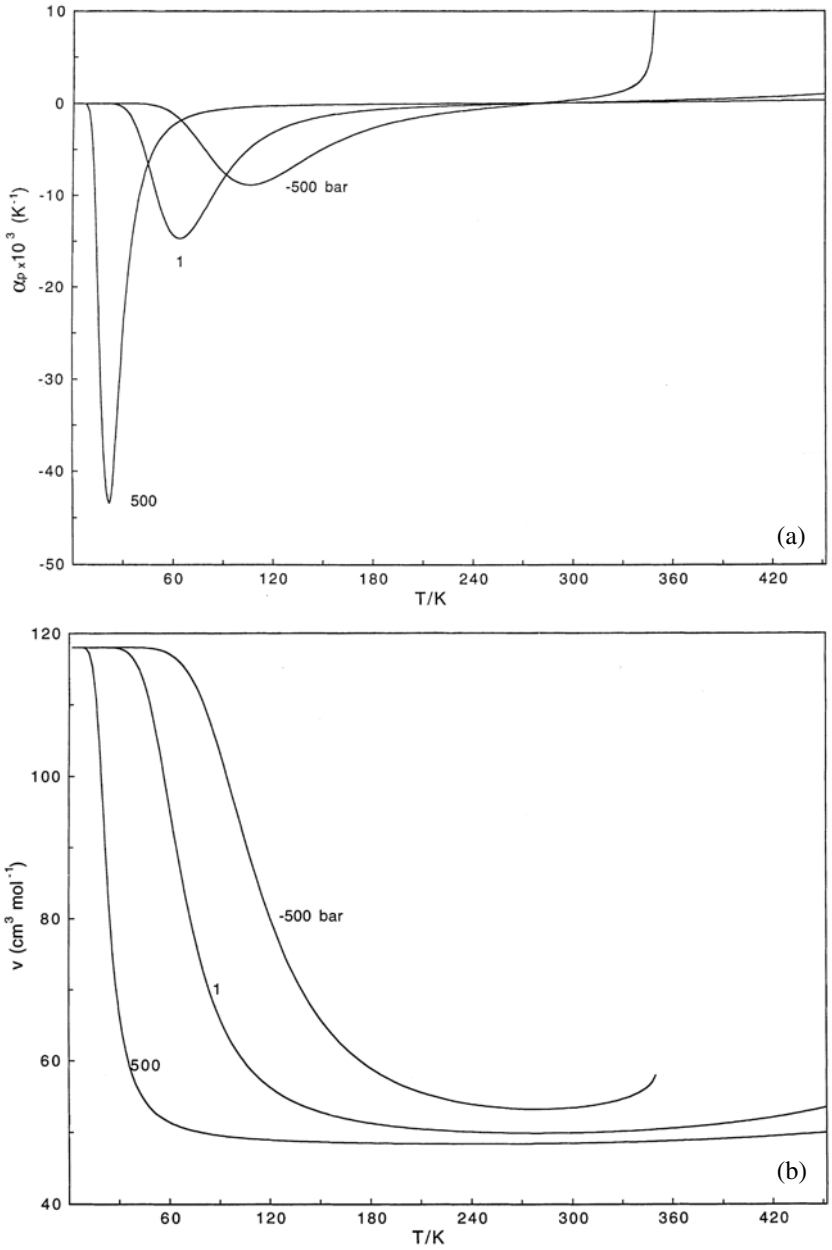

Figure 28. Temperature dependences of the thermal expansion coefficient (a) and molar volume (b) at various pressures for the mean-field solution of the water-like lattice model of Sastry *et al* [16, 258]. Note that the volume changes upon isobaric cooling are continuous. These changes become more abrupt upon increasing the pressure, and they then occur at progressively lower temperatures. These calculations illustrate the singularity-free scenario. Reprinted, with permission, from [258].

Figure 29 illustrates the general features of the singularity-free scenario, as predicted by the model of Truskett *et al* [221]. With an appropriate choice of parameters, this model is capable of reproducing both the singularity-free (figure 29) and the two-critical-point scenarios

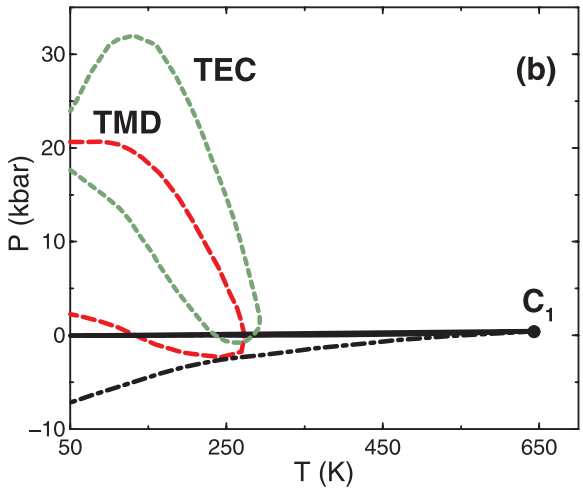

Figure 29. The singularity-free scenario as illustrated by the microscopic model of associating fluids of Truskett *et al* [221]. C1 is the vapour–liquid critical point, the full line is the boiling curve and the dot–dashed line is the liquid spinodal. Water-like anomalies exist in the absence of a low-temperature transition. TMD is the locus of density extrema, and it encloses the region where the thermal expansion coefficient is negative. TEC is the locus of compressibility extrema, which bounds the region where the compressibility increases upon isobaric cooling. The high- and low-temperature branches of the TEC locus are loci of compressibility minima and maxima with respect to temperature along isobars, respectively. Reprinted, with permission, from [221].

(see figure 2 of [221]). The important point of figures 28 and 29 is not the specific model used in the calculations but the overall behaviour, which, like the two-critical-point scenario, is thermodynamically consistent and explains the experimental observations. None of the theoretical models discussed in sections 7.2 and 7.3 is realistic and accurate enough to have predictive value. Hence calculations such as those shown in figures 27–29 are of value not because they constitute accurate predictions (which they do not), but because they show a thermodynamically consistent interpretation of the phase behaviour of metastable water. Identifying which of these scenarios applies to water is the task of experiments.

In principle, answering this question should not be difficult. A system quenched rapidly into the presumed coexistence region should phase separate. If on the other hand there is no phase transition, the system would remain indefinitely stable. In practice, however, non-crystalline water is a glass, not a liquid, over much of the experimentally accessible temperature range of interest. The extraordinarily slow structural relaxation rates involved stand in the way of simple quenching experiments. Direct, real-time measurements on droplets small enough (and cooled fast enough) to avoid crystallization would in principle yield the information needed to distinguish between the two scenarios. So far, this challenge has not been met.

7.4. Other interpretations

The interpretations discussed so far are based on thermodynamic arguments. In contrast, Tse and co-workers [152, 165] have argued that the pressure-induced amorphization of ice Ih is the result not of an equilibrium thermodynamic transformation but of a mechanical instability. Using molecular dynamics simulation of the TIP4P potential [201], Tse [165] observed a sharp decrease of the elastic moduli of ice Ih after 20 ps at 80 K and 9 kbar. The necessary condition for the mechanical stability of the crystal lattice, namely the requirement that the energy must be a minimum with respect to small deformations, can be expressed in terms of

inequalities involving the elastic moduli, also known as the Born stability criteria [263]. Tse showed that two of the three Born inequalities were close to being violated following the sharp decrease of the elastic constants, although no actual stability violation occurred. In a subsequent study, Tse *et al* [152] performed lattice dynamics calculations on the TIP4P potential and showed that the mechanical and thermodynamic melting lines intersect at ∼160 K, and argued that the mechanism for the pressure-induced amorphization changes from thermodynamic for $T > 160$ K to mechanical at lower temperatures. The thermodynamic melting line was not computed form the free energies of the coexisting phases; instead, the empirical Lindemann criterion [264] was used. It is possible, as argued by Tse and co-workers, that the mechanism of pressure-induced amorphization of ice Ih into HDA may involve a mechanical instability rather than equilibrium melting, especially at low temperatures[4]. It is also true that a transition involving a glassy phase does not proceed via a reversible path. But the existence of kinetic barriers should not be invoked to rule out the relevance of underlying thermodynamic driving forces. This is especially important in the case of supercooled water, so many of whose anomalies are thermodynamic.

An alternative interpretation of the HDA–LDA transformation has been proposed recently[5] [180]. Using neutron and x-ray diffraction, Tulk *et al* followed the evolution of the first diffraction peak of recovered (atmospheric pressure) HDA upon annealing at 95, 100, 105 and 110 K. The position of this peak evolves through a series of distinct intermediate states. The authors interpreted their results as implying that the transition from HDA to LDA can proceed in a structurally continuous manner through a series of intermediate amorphous forms, and that, therefore, 'phase transformations in low-temperature liquid water may be much more complex than currently understood'. Since a reversible transition between HDA and LDA requires temperatures of at least 130 K [172], the observed behaviour is fully consistent with incomplete structural relaxation upon annealing at different temperatures. These results neither suggest nor require a reinterpretation of the HDA–LDA transformation.

The glass transition temperature of HGW and ASW (136 ± 1 K) [28, 158] is slightly different from that of LDA (129 ± 2 K) [153, 157] (see table 7). Johari *et al* [153] have argued that the viscous liquids that result on thermal cycling of these amorphous phases up to 148 K are calorimetrically distinct forms of liquid water. Water A results upon heating ASW or HGW, and water B results upon heating LDA. Thermal cycling of HGW or ASW, on the one hand, and LDA, on the other, up to 148 K, followed by cooling and re-heating, gave rise to the same glass transition temperatures (136 K for HGW/ASW and 129 K for LDA). Johari *et al* then concluded that water A and B are not interconvertible through a reversible path, that water A is thermodynamically continuous with supercooled water and that water B 'is a new phase whose incorporation in a phase diagram requires further experiments'. This interpretation hinges on the assumption that the material that results upon heating ASW or HGW and LDA above 148 K is an equilibrated liquid. The evidence on this is not definitive, data having been interpreted both in support of [50] and against [161] the notion of a highly viscous but equilibrated liquid at $T < 150$ K. In the light of this, and of the current debate surrounding water's glass transition temperature [8, 30, 162, 163], it appears simpler to regard the interesting observations of Johari *et al* [153] as suggesting that the product of heating LDA and ASW across their 'glass transition' may not be a fully equilibrated liquid. This obviates the necessity of invoking yet another phase of water.

Speedy [265] proposed the existence of a new phase of water, which he called water II. Speedy's argument was based on the thermodynamic constraints that ensue from the existence

[4] As mentioned in section 6.2, though, the fact that no microcrystallinity was detected in a recent neutron diffraction study of HDA [166] casts doubt on this viewpoint.

[5] See also section 6.3.

of a reversible isobaric path connecting states of water at 236 K (T_2) and 150 K (T_1) at atmospheric pressure. At 236 K liquid water is supercooled, and this is an easily attainable experimental condition. 150 K marks the onset of spontaneous crystallization to cubic ice (Ic). It follows, from the fact that the heat capacity of the metastable liquid is larger than that of the corresponding crystal at the same temperature and pressure, that

$$\Delta s(T_1) \leqslant \Delta s(T_2) - [\Delta h(T_2) - \Delta h(T_1)]/T_2 \tag{18}$$

where Δ denotes property differences between metastable (non-crystalline) water and ice Ih at the same temperature and pressure. All of the quantities in the right-hand side have been measured, and one obtains therefore [265]

$$\Delta s(T_1) \leqslant 2.9 \text{ J K}^{-1} \text{ mol}^{-1}. \tag{19}$$

Speedy argued that inequality (19) constrains the entropy difference at 150 K to being unreasonably small, and that accordingly there is no reversible path connecting non-crystalline water at 150 K to supercooled water at 236 K. The amorphous material at 150 K is therefore, according to Speedy, a new phase of water, which he called water II [265]. The basis for this assertion is a theoretical estimate of $\Delta s(0)$ [134, 266]. Using this theoretical value, and correcting to 150 K using estimates for the heat capacity difference between the glass and the crystal, Speedy concluded that 2.9 J mol^{-1} K^{-1} is too small an entropy difference between glassy and crystalline water. The problem with this argument is the *a priori* assumption that the theory is correct. A subsequent experimental determination of $\Delta s(T_1)$ by Speedy *et al* based on evaporation rate measurements of amorphous and crystalline water films [160] has in fact confirmed the validity of inequality (19), and thereby shown that it is not necessary to invoke discontinuities [267, 268] between supercooled and glassy water.

In an interesting series of papers, Kiselev [269] and Kiselev and Ely [270–272] have examined critically the experimental significance of a possible second critical point. They developed a crossover equation for liquid water based on the fluctuation theory of critical phenomena, which predicts a second critical point at 188 K and 230 MPa [271]. They then compared the lifetime of metastable liquid states with the characteristic time required to attain local equilibrium. Their thought-provoking conclusion is that the second critical point lies in a 'non-thermodynamic habitat' in which the lifetime of the metastable state is shorter than the time required for the attainment of internal equilibrium. The work of Kiselev and Ely points to the need to evaluate critically the meaning of a thermodynamic state at very large degrees of metastability. The recent computational study of deeply supercooled TIP5P water [210] by Yamada *et al* [211] has addressed this question, and shown that, at least for this model, thermal equilibrium is in fact attained in the region of the liquid–liquid transition.

7.5. Dynamics

The stability limit conjecture is a thermodynamic theory. Nevertheless, power-law fits to supercooled water's dynamic properties, such as equation (7), based on the existence of a pressure-dependent singular temperature $T_s(P)$ have been used as well (e.g., [60, 127]). In their seminal 1976 paper [60], where the existence of an underlying singularity was first postulated, Speedy and Angell showed that measurements of water's viscosity, diffusion coefficient, dielectric relaxation time, and proton and oxygen spin–lattice relaxation times could be accurately fitted with the power-law expression

$$\tau = \tau_0(T/T_s - 1)^{-\gamma} \tag{7}$$

where τ is a characteristic relaxation time (e.g., D^{-1}). As shown in figure 15, equation (7) describes supercooled water's relaxation behaviour at pressures below 1.5 kbar. There

is, however, no established theoretical basis for diverging relaxation times at the spinodal curve, except at the critical point. Furthermore, homogeneous nucleation of ice precludes measurements close enough to the presumed singular temperature to make such power-law fits unambiguous. The Speedy–Angell fits highlighted the unusual behaviour of supercooled water's relaxation dynamics. However, the underlying cause of this behaviour is not necessarily thermodynamic, and it was not until twenty years after the Speedy–Angell paper was published that a plausible interpretation of a dynamic singularity was proposed.

In an important body of computational work, Gallo *et al* [273], Sciortino *et al* [274, 275] and Sciortino [276] showed that the SPC/E model of water [216] exhibits slow dynamics in the supercooled region that is consistent with the predictions of the idealized mode-coupling theory [277]. Mode-coupling theory provides an accurate description of the temporal evolution of correlation functions that have non-zero overlap with the density. It predicts that a purely dynamic structural arrest occurs at a temperature $T_c(P)$, below which the correlation functions no longer decay to zero. In reality, the coupling between density and momentum fluctuations, which is not taken into account in the so-called idealized mode-coupling theory, restores ergodicity below T_c. It is now understood that the predictions of the idealized mode-coupling theory are applicable to the moderately supercooled regime. Sciortino and co-workers [273–275] showed that at -80 MPa (the pressure at which the density along the TMD is 1 g cm^{-3} in the SPC/E model) an idealized (hence extrapolated) mode-coupling transition occurs at a temperature $T_c(P)$ that is 50 K below SPC/E's TMD. Although SPC/E water remains ergodic below T_c, its slow dynamics is dominated by the proximity to this avoided singularity. Significantly, the Speedy–Angell singular temperature [60] at which power-law fits of transport properties appear to diverge at atmospheric pressure, 228 K, is also 49 K below the TMD. Thus, the main significance of the simulation work of Sciortino and co-workers is that it provides a plausible interpretation based on the idea of a purely dynamic origin for several of supercooled water's anomalies. According to this view, no thermodynamic singularity is needed in order to explain the slowing down of structural relaxation in supercooled water. Rather, an avoided dynamic transition where the system would become non-ergodic is thought to underlie the experimental observations of slow dynamics in supercooled water.

Figure 30 shows the mean squared displacement of the centre of mass of water molecules as a function of time, for simulated temperatures between 206.3 and 284.5 K, at approximately isobaric conditions corresponding to a negative pressure of about -80 MPa. It can be seen that at sufficiently low temperatures an intermediate regime appears between the ballistic ($\langle(\delta r)^2\rangle \sim t^2$) and diffusive regimes ($\langle(\delta r)^2\rangle \sim t$). During this intermediate time the mean squared displacement remains almost flat. At sufficiently low temperatures, molecules appear to be trapped in cages for increasingly longer periods of time, during which they execute localized motions and are not able to diffuse. Figure 31 shows the time dependence of the self-intermediate scattering function for the centre-of-mass motion over the time interval $10^{-3} < \tau < 10^4$ ps, at the same conditions as in figure 30, and for a wavevector q corresponding to the peak of the structure factor. The quantity plotted in figure 31 is the space Fourier transform of the van Hove self-correlation function, $G_s(\mathbf{r}, t)$:

$$G_s(\mathbf{r}, t) = \frac{1}{N}\left\langle \sum_{i=1}^{N} \delta(\mathbf{r} + \mathbf{r}_i(0) - \mathbf{r}_i(t)) \right\rangle \tag{20}$$

where δ denotes the Dirac delta function, $\mathbf{r}_i(t)$ is the centre-of-mass position of molecule i at time t, and N is the number of molecules in the system. The quantity $4\pi r^2 G_s \, dr$ is the probability that a molecule is at a distance r from the origin at time t, given that it was at the origin at time 0.

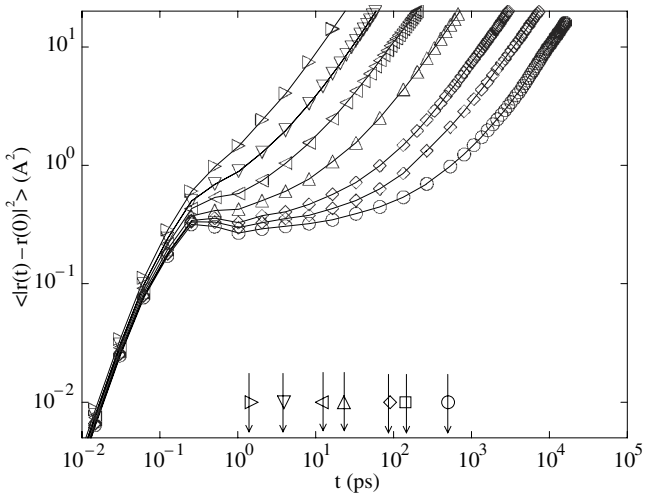

Figure 30. The mean squared displacement of the centre of mass of SPC/E water molecules as a function of time for simulated temperatures of 206.3 K (○), 209.3 K (□), 213.6 K (◇), 224 K (△), 238.2 K (◁), 258.5 K (▽) and 284.5 K (▷). Note the cage effect, starting at about 0.25 ps, followed by free diffusion. The arrows indicate the time at which an indicator of deviations from Gaussian behaviour in the distribution of particle displacements reaches its maximum value. Reprinted, with permission, from [274] Sciortino F *et al* 1996 *Phys. Rev.* E **54** 6331. Copyright (1996) by the American Physical Society.

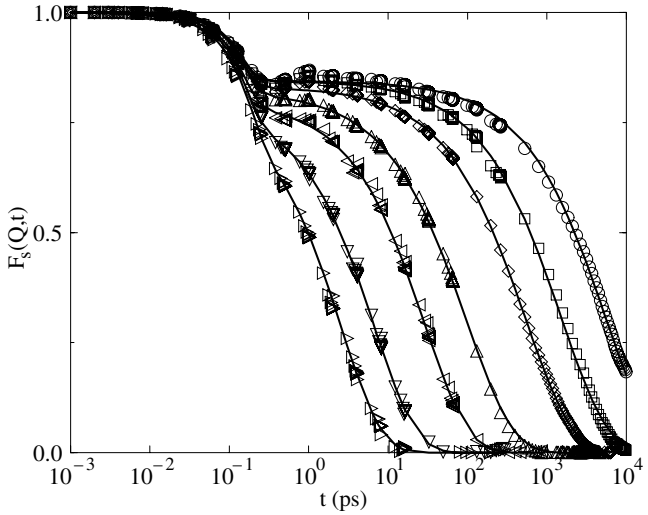

Figure 31. Time evolution of the self-intermediate scattering function for SPC/E water molecules. The simulated temperatures and symbols are the same as in figure 30. The calculations are for a wavevector corresponding to the first peak of the structure factor. Note the two-stage relaxation at low temperatures, with β and α regimes corresponding to the approach to, and initial departure from, the plateau. Reprinted, with permission, from [274] Sciortino F *et al* 1996 *Phys. Rev.* E **54** 6331. Copyright (1996) by the American Physical Society.

The decay of the scattering function exhibits three regimes: an initial fast decay, an intermediate plateau and long-time relaxation. The entire decay was well fitted with the

function

$$F_s(Q,t) = [1 - A(Q)]e^{-(t/\tau_s)^2} + A(Q)e^{-(t/\tau_l)^\beta} \tag{21}$$

where $A(Q)$ is the Debye–Waller factor; τ_s and τ_l are the short- and long-term relaxation times, and β (<1) is the stretch exponent. The existence of the three regimes of structural relaxation shown in figure 31 is an important prediction of the so-called idealized mode-coupling theory [277]. The theory makes specific predictions about the functional form of $F(t)$, both as it approaches and departs from the intermediate plateau (β and α regimes, respectively). For isobaric conditions, these predictions read:

$$F_s(Q,t) - A(Q) = B_Q(t/t_0)^{-a} \tag{22}$$

$$F_s(Q,t) - A(Q) = -C_Q(t/\tau)^{-b} \tag{23}$$

$$\tau = t_0(T/T_c(P) - 1)^{-(1/2b+1/2a)} \tag{24}$$

$$D^{-1} \propto [T/T_c(P) - 1]^{-\gamma} \tag{25}$$

$$\gamma = \frac{1}{2a} + \frac{1}{2b} \tag{26}$$

$$\frac{[\Gamma(1-a)]^2}{\Gamma(1-2a)} = \frac{[\Gamma(1+b)]^2}{\Gamma(1+2b)}. \tag{27}$$

Equations (22) and (23) describe the approach to (β relaxation) and initial departure from (α relaxation) the intermediate plateau, $A(Q)$. The theory predicts that both are described by power laws, with exponents a and b, where t_0 is a characteristic microscopic relaxation time. The exponents a and b are not independent, but are instead related through the transcendental equation (27), where Γ denotes the gamma function. γ in equations (25) and (26) is the exponent that governs structural arrest as the system approaches the singular temperature $T_c(P)$ along an isobaric path. Using the simulation results shown in figure 31 and the theoretical predictions (22)–(27), Sciortino and co-workers obtained a singular temperature of 199 K. Significantly, this temperature is approximately 50 K lower than the TMD for the SPC/E model at the pressure considered in their study. For water at atmospheric pressure, the Speedy–Angell extrapolated singular temperature, 228 K, is also 50 K below the TMD. The theoretical prediction that $A(Q)$, B_Q and C_Q are temperature independent was verified.

In subsequent related work, Starr *et al* [278, 279] investigated the low-temperature dynamics of the SPC/E model under pressure, up to 25 kbar. They also analysed their results within the framework of mode-coupling theory, and obtained a $T_c(P)$ locus in qualitative agreement with the one predicted by power-law extrapolation of NMR spin-echo measurements by Prielmeier *et al* [19]. A significant difference between SPC/E and real water noted by Starr *et al* is that the diffusivity maxima as a function of pressure are more pronounced and occur at higher pressures in SPC/E than in real water. Also, the exponent γ characterizing the (extrapolated) vanishing of the diffusivity increases with pressure in water, and decreases with pressure in SPC/E.

The work of Sciortino and co-workers [273–276] and of Starr *et al* [278, 279] gives support to the notion that mode-coupling theory captures the main features associated with the slowing down of water dynamics between the freezing and homogeneous nucleation temperatures. Their results and analysis suggest that the sharp increase in relaxation times pointed out by Speedy and Angell [60] can be explained without invoking thermodynamic interpretations. The underlying physical picture is one in which slow dynamics arises as a result of transient caging of molecules, as evidenced by the intermediate-time plateaus in figures 30 and 31. This apparent success of the idealized mode-coupling theory is rather surprising. In the first place, the dynamics of SPC/E are consistent with the mode-coupling predictions over a very broad

range of pressure, where the primary controlling factor for the mobility changes gradually form hydrogen bonding at low pressure to excluded volume at high pressures. Secondly, the idealized mode-coupling theory was not formulated for network-forming fluids interacting through directional forces. Instead, it is strictly applicable to simple, atomic systems. Fabbian *et al* have subsequently extended mode-coupling theory to molecular liquids, including water [280–282]. Comparison between theoretical predictions and simulations supports the applicability of mode-coupling theory to the description of dynamics in moderately supercooled molecular liquids.

In contrast to the results of Sciortino and co-workers for SPC/E water, Patschek and Geiger [283] studied the dynamics of the ST2 model in the supercooled region along the 80 MPa isobar, and found no evidence of structural arrest. Instead, these authors found an evolution from continuum to jump-like diffusion at low temperatures, and a corresponding change in the activation energy for diffusion, which reached a value of 115 kJ mol^{-1} below about 285 K. This value is close to four times the energy of a hydrogen bond. The diffusivity was found to exhibit Arrhenius behaviour both at high and low temperatures, albeit with very different activation energies. This discrepancy between the SPC/E and ST2 results is not well understood. One possible explanation hinges on the fact that the ST2 potential gives rise to a more structured liquid than does SPC/E, and hence anomalous behaviour tends to be shifted up in temperature with respect to experiments in the former case, and downwards in the latter. Hence kT may be large enough to activate a significant fraction of molecular jumps when cages begin to form in ST2 water, preventing the observation of the approach to the kinetic glass transition [276]. Clearly, a systematic investigation of supercooled dynamics for various water models is needed.

Starr *et al* [284] investigated theoretically the dynamic properties of deeply supercooled water in the range 136 K $\leqslant T \leqslant$ 235 K—that is to say, between the glass transition and homogeneous nucleation temperature. Their approach is based on the Adam–Gibbs theory of relaxation in supercooled liquids [285]. According to this theory, the relaxation time satisfies

$$\tau = \tau_0 \exp(A/Ts_{\mathrm{conf}}) \tag{28}$$

where τ is a characteristic relaxation time (e.g., the viscosity); τ_0 and A are temperature-independent constants; and s_{conf} is the molar configurational entropy. The configurational entropy is that part of the entropy due to the system's potential energy [285]. The Adam–Gibbs theory has proved remarkably successful in correlating experimental data on relaxation in supercooled liquids (e.g., [286]), and in such cases s_{conf} is commonly interpreted as the entropy difference between the supercooled liquid and the stable crystal at the same temperature and pressure (henceforth referred to as excess entropy). This interpretation is based on a topographic view of supercooled liquids and glasses [287], according to which molecular motion in such systems can be decomposed into sampling distinct potential energy minima (configurational) and thermal vibrations about a given deep minimum (vibrational). Since only the latter exist in crystals, and if one assumes further that the vibrational entropies of the supercooled liquid and the crystal are equal, then the difference in entropy between liquid and crystal is equal to the configurational entropy. The validity of equation (28) has also been corroborated in computer simulations (e.g., [288]), with s_{conf} calculated as the difference between the total and vibrational entropies (e.g., [289]).

Starr *et al* [284] estimated the transport properties of deeply supercooled water assuming the validity of the Adam–Gibbs theory. Knowledge of the excess Gibbs free energy, entropy, and isobaric heat capacity at 150 (T_{X}) and 236 K (T_{H}) places five constraints on the excess entropy function, namely the value of the function and of its first derivative at the two end

points, and the integral of the function:

$$s_{\mathrm{ex}}(T_{\mathrm{X}}), \qquad s_{\mathrm{ex}}(T_{\mathrm{H}}) \tag{29}$$

$$c_{p,\mathrm{ex}}(T_{\mathrm{X}}) = T_{\mathrm{X}}\left(\frac{\partial s_{\mathrm{ex}}}{\partial T}\right)_{p,T=T_{\mathrm{X}}}, \qquad c_{p,\mathrm{ex}}(T_{\mathrm{H}}) = T_{\mathrm{H}}\left(\frac{\partial s_{\mathrm{ex}}}{\partial T}\right)_{p,T=T_{\mathrm{H}}} \tag{30}$$

$$\int_{T_{\mathrm{X}}}^{T_{\mathrm{H}}} s_{\mathrm{ex}}\,\mathrm{d}T = g_{\mathrm{ex}}(T_{\mathrm{X}}) - g_{\mathrm{ex}}(T_{\mathrm{H}}) = [h_{\mathrm{ex}}(T_{\mathrm{X}}) - T_{\mathrm{X}}s_{\mathrm{ex}}(T_{\mathrm{X}})] - [h_{\mathrm{ex}}(T_{\mathrm{H}}) - T_{\mathrm{H}}s_{\mathrm{ex}}(T_{\mathrm{H}})]. \tag{31}$$

Using experimental values of the excess heat capacity, entropy and enthalpy, and the assumption that the excess heat capacity is non-singular in the temperature interval of interest, Starr *et al* constructed plausible forms for the temperature-dependent excess entropy and fitted experimental data for viscosity at $T > T_{\mathrm{H}}$ to equation (28), to yield the undetermined constants τ_0 and A. They used the sum of excess and residual entropies in their calculations:

$$s_{\mathrm{conf}} \approx s_{\mathrm{ex}} + s_{\mathrm{res}}. \tag{32}$$

The residual entropy is that part of the entropy of ice due to proton disorder [290]. The predicted diffusivity and viscosity are shown in figure 32. Note the change from an $\eta(T)$ functionality that displays super-Arrhenius (fragile) behaviour at high temperature (positive curvature in $\ln \eta$ versus $1/T$ coordinates; that is to say, effective activation energy that increases upon cooling) to quasi-Arrhenius (strong) behaviour below $T \approx 190$ K (linear $\ln \eta$ versus $1/T$ functionality). In terms of Angell's useful classification scheme for glass-forming liquids, water is predicted to undergo a fragile-to-strong transition in the deeply supercooled region [291].

The prediction of a fragile-to-strong transition in deeply supercooled water is not supported by the data of Smith and Kay [49] shown in figure 13. Smith and Kay were able to fit their diffusivity data with a VTF form, $D = D_0 \exp[-B/(T - T_0)]$, with a singular temperature $T_0 = 118$ K. This discrepancy can be seen quite dramatically in figure 32, which includes the measurements of Smith *et al* [114] as open squares. The reasons for this failure of the theory to reproduce experimental measurements are not well understood. Whether this reflects the breakdown of the Adam–Gibbs equation in deeply supercooled water (although the validity of the Adam–Gibbs equation for the supercooled SPC/E model of water has been verified [292]) or more generally the presence of a Kiselev–Ely 'non-thermodynamic habitat' [269–272] where thermal equilibrium cannot be attained is an interesting question that deserves further attention.

At present, therefore, there are two mutually exclusive interpretations of the dynamics of supercooled water, which can be summarized as follows. The diffusivity measurements of Smith and Kay [49] in the range 150–157 K are smoothly connected to the 'high'-temperature data for supercooled water [19, 107] above the homogeneous nucleation temperature. No singularity near 228 K occurs in this representation, according to which water is a normal fragile liquid in the vicinity of 150 K. This 'singularity-free' view of relaxation is supported by simulation results for the ST2 model [283]. In contrast, water's orientational relaxation times above the homogeneous nucleation temperature and below about 1.5 kbar can be accurately fitted with a power-law functionality that includes a pressure-dependent singular temperature where the extrapolated relaxation times diverge [125]. This singular temperature (223 K at 1 bar) is very close to the Speedy–Angell temperature, 228 K. This view is supported by simulations of the SPC/E model [273–276, 278, 279], which clearly show an underlying *avoided* dynamic singularity, identified as the mode-coupling 'critical' temperature. In this alternative view, water's relaxation dynamics changes somewhere between 220 and 230 K (atmospheric pressure), and an avoided singularity separates high-temperature fragile behaviour from low-temperature strong behaviour. This view is consistent with the Adam–Gibbs-based calculations of Starr *et al* [284], although no explicit mention is made in the latter of an avoided singularity.

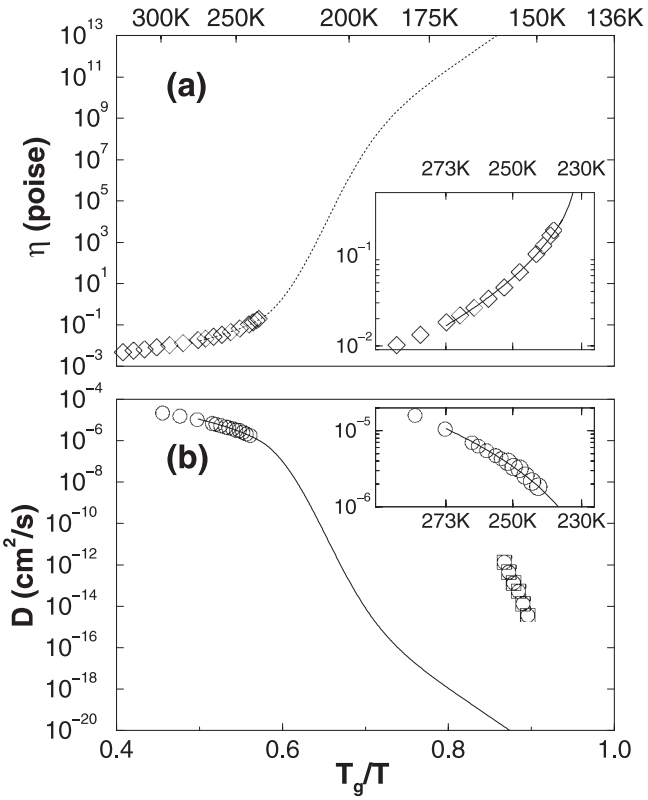

Figure 32. The temperature dependence of the viscosity (a) and self-diffusion coefficient (b) of supercooled water. Data points in the moderately supercooled region ((◇) [120, 122]; (○) [107]) are shown, both in the main panels and in detail in the insets, along with theoretical predictions (dotted and full lines) based on the validity of the Adam–Gibbs equation (25) and calculated configurational entropy, constrained by experimental data as explained in the text. The data of Smith and Kay (□) [49] are also shown, illustrating the large gap between theoretical predictions and experiments. Reprinted, with permission, from [284] Starr F W *et al* 2003 *Physica* A **323** 51. Copyright (2003), with permission from Elsevier.

The dynamics of supercooled water has also been interpreted in terms of the topography of its multidimensional potential energy surface, also referred to as its energy landscape (e.g., [287]). This refers to the surface generated by a system's potential energy as a function of its degrees of freedom (e.g., particle coordinates for an atomic fluid). The energy landscape formalism (e.g., [293]) provides a useful framework for describing the static and dynamic properties of supercooled liquids and glasses. Scala *et al* [292] found a close relation between diffusion and configurational entropy in the SPC/E model. The configurational entropy is that part of the system's entropy that arises from the sampling of different potential energy minima [289]. La Nave *et al* [294] found a strong relationship between diffusion and the fraction of negative eigenvalues of the Hessian matrix that correspond to transitions between adjacent potential energy minima. Giovambattista *et al* [295] found an intriguing inverse relationship between the average cluster size of mobile supercooled SPC/E water molecules and the configurational entropy associated with the degeneracy of potential energy minima. Taken together, these investigations suggest a view of water's slow dynamics in the moderately supercooled regime in which diffusion is controlled by the topography of the potential energy landscape [296]. Perhaps the most intriguing observation from these studies is the existence

of a relationship between the number of potential energy minima [292] and the connectivity between them [294]. This has important theoretical implications for the theory of glasses and supercooled liquids in general, not just for water. In particular, establishing a formal connection between the energy landscape view and mode-coupling theory remains a challenge.

The computational study of SPC/E water by Errington and Debenedetti [21] identified a common structural cause underlying both dynamic and thermodynamic anomalies in cold liquid water. By tracking the evolution of metrics for orientational and translational order over broad ranges of temperature and density, including the deeply supercooled region, these authors showed that SPC/E water's anomalies occur as a cascade, as a result of progressive structural ordering upon cooling and decompression. Equilibrium states with thermodynamic anomalies ($\alpha < 0$) are also necessarily states where the diffusivity D increases upon isothermal compression (anomalous transport behaviour), whereas the converse is not true. Thus, the dome-like region in the (T, ρ) plane where $\alpha < 0$ was found by Errington and Debenedetti to lie entirely inside the $\mathrm{d}D/\mathrm{d}\rho > 0$ dome. The fact that the orientational and translational metrics are correlated throughout the anomalous region allowed Errington and Debenedetti to quantify the degree of structural order in SPC/E water and to calculate the minimum degree of order needed to trigger the various anomalies. These ideas have yet to be applied to water's many other anomalous properties, as well as to other water models.

8. Conclusions

Slightly more than two decades have elapsed since Speedy proposed his stability limit conjecture [184] and Angell wrote his now classic reviews on supercooled water [6, 7]. This has been a period of explosive growth in interest and knowledge on the topic. The most important development has been the discovery of polyamorphism in water [150]. The sharpness and apparent reversibility of the transition between LDA and HDA inspired an important body of work aimed at exploring, theoretically and computationally, the notion of a first-order transition between distinct liquid phases of a pure substance. There has resulted a vastly broadened perspective on the liquid state of matter [194, 195, 297, 298].

The experimental study of glassy water has added significantly to the body of empirical and factual knowledge on this most important of substances. Nevertheless, and in spite of impressive progress in measurement, modelling and simulation, large gaps in our understanding of the global phase behaviour and the relaxation dynamics of cold, non-crystalline, metastable water still remain. The key unanswered questions are:

Does water possess a second critical point?

There are two thermodynamically consistent scenarios that can account for the known experimental facts concerning supercooled water. One of them posits the existence of a metastable critical point around 220 K and 1 kbar [203]. Proving or disproving the existence of this critical point—that is to say, distinguishing between the second-critical-point and singularity-free interpretations—is the single most important goal as regards metastable water's phase behaviour. The preponderance of evidence favours the two-critical-point interpretation [178, 203, 204]. Small droplets and molecular clusters [43–48] appear promising systems in which to pursue further investigation of this question. Theoretically and computationally, a more systematic understanding of what types of intermolecular interaction promote liquid–liquid immiscibility, both in the absence and in the presence of density anomalies, is desirable.

Can the first question be answered by experiments?

The interesting work of Kiselev and Ely [269–272] raises the question of whether the very notion of a thermodynamic state retains significance deep enough inside the metastable region. This is a topic that deserves more attention than it has received so far. Experimental knowledge of structural relaxation dynamics in water in the 140–230 K range is urgently needed. More computational studies of structural relaxation in deeply supercooled realistic water models, such as [211], should also prove useful. The more general theoretical question of how to rigorously incorporate metastability into statistical mechanics remains a challenge, interesting steps in this direction notwithstanding (e.g., [299–302]). Valuable insight may also result from comparisons with other systems in which polyamorphic transitions occur (see, e.g., [194, 195, 297, 298]). The latter is a rich avenue of research not discussed in this review, which is limited exclusively to water.

Is non-crystalline water a liquid at atmospheric pressure and in the temperature range from 140 to 150 K?

In the approximate temperature range 140–150 K water may be hot enough to be no longer a glass, yet cold enough to be not yet able to crystallize at a measurable rate. This should allow additional measurements of transport and flow properties to be made (e.g., [49, 50]) so as to clarify the nature of water's low-temperature non-crystalline state. The preponderance of evidence suggests that water is indeed a very viscous liquid under these conditions [49, 50], but challenges to this viewpoint [7, 161] have not been conclusively disproved.

Is there a transition from fragile to strong behaviour in supercooled water?

The diffusivity measurements of Smith and Kay [49], and the ST2 simulations of Patschek and Geiger [283] suggest that supercooled water is a fragile liquid slightly above 150 K, and that the dynamics of supercooled water above the homogeneous nucleation temperature is smoothly connected to that of the ultraviscous liquid above T_g. In contrast, the NMR measurements of Lang and Lüdemann [125] and the SPC/E simulations of Sciortino *et al* [274, 275], Gallo *et al* [273] and Starr *et al* [278, 279] are consistent with an *avoided* singularity near 228 K and a gradual change in water dynamics from fragile behaviour above the singularity temperature to strong behaviour below. Resolution of this question requires experimental measurements of relaxation dynamics in the 140–230 K range, as well as systematic computational studies of supercooled dynamics for several realistic water models across broad ranges of temperature and pressure.

Is VHDA a distinct form of amorphous water?

VHDA's overall significance with respect to metastable water's phase behaviour is not yet understood. In particular, it is not known with certainty whether VHDA is a distinct phase, separated from HDA by a first-order transition, or whether it is simply very dense HDA.

Seeking answers to these questions is important not just for an improved understanding of water. The known implications of this research impact on biology (e.g., [303, 304]), astronomy and planetary science (e.g., [305–308]), atmospheric science (e.g., [40–42]) and pharmaceutical processing (e.g., [309]). Others still are likely to emerge, as deeper knowledge is gained about the properties of water outside its normal range of stability.

Acknowledgments

I am grateful to Austen Angell, Osamu Mishima, Giancarlo Ruocco, Francesco Sciortino and Gene Stanley for their very helpful comments, to Tom Truskett for providing figure 3, and to the US Department of Energy's Office of Basic Energy Sciences for its generous support of my research on supercooled water.

References

[1] Franks F 2000 *Water: a Matrix for Life* 2nd edn (Cambridge: Royal Society of Chemistry)
[2] Ball P 2000 *Life's Matrix: a Biography of Water* (New York: Farrar, Straus, and Giroux)
[3] Debenedetti P G and Stanley H E 2003 *Phys. Today* **56** (6) 40
[4] Petrenko V F and Whitworth R W 1999 *Physics of Ice* (Oxford: Oxford University Press)
[5] Lobban C, Finney J L and Kuhs W F 1998 *Nature* **391** 268
[6] Angell C A 1983 *Annu. Rev. Phys. Chem.* **34** 593
[7] Angell C A 1982 *Water—a Comprehensive Treatise* vol 7, ed F Franks (New York: Plenum) chapter 1
[8] Angell C A 2002 *Chem. Rev.* **102** 2627
[9] Zannotti J-M, Bellissent-Funel M-C and Chen S-H 1999 *Phys. Rev.* E **59** 3084
[10] Gallo P, Rovere M and Spohr E 2000 *Phys. Rev. Lett.* **85** 4317
[11] Koga K, Tanaka H and Zeng X C 2000 *Nature* **408** 564
[12] Eisenberg D and Kauzmann W 1969 *The Structure and Properties of Water* (Oxford: Clarendon)
[13] Pauling L 1970 *General Chemistry* (New York: Dover)
[14] Stillinger F H 1980 *Science* **209** 451
[15] Rowlinson J S and Swinton F L 1982 *Liquids and Liquid Mixtures* 3rd edn (London: Butterworth)
[16] Sastry S, Debenedetti P G, Sciortino F and Stanley H E 1996 *Phys. Rev.* E **53** 6144
[17] Lifshitz E M and Pitaevskii 1980 *Statistical Physics* part 1, 3rd edn (Oxford: Pergamon)
[18] DeFries T and Jonas J 1977 *J. Chem. Phys.* **66** 896
[19] Prielmeier F X, Lang E W, Speedy R J and Lüdemann H-D 1988 *Ber. Bunsenges. Phys. Chem.* **92** 1111
[20] Stanley H E and Teixeira J 1980 *J. Chem. Phys.* **73** 3404
[21] Errington J R and Debenedetti P G 2001 *Nature* **409** 318
[22] Mishima O and Stanley H E 1998 *Nature* **396** 329
[23] Apfel R E 1972 *Nature Phys. Sci.* **238** 63
[24] Debenedetti P G 1996 *Metastable Liquids. Concepts and Principles* (Princeton, NJ: Princeton University Press)
[25] Skripov V P and Pavlov P A 1970 *High Temp. (USSR)* **8** 782
[26] Cwilong B M 1947 *Proc. R. Soc.* A **190** 137
[27] Mossop S C 1955 *Proc. Phys. Soc.* B **68** 193
[28] Johari G P, Hallbrucker A and Mayer E 1987 *Nature* **330** 552
[29] Hallbrucker A, Mayer E and Johari G P 1989 *J. Phys. Chem.* **93** 4986
[30] Velikov V, Borick S and Angell C A 2001 *Science* **294** 2335
[31] Hallbrucker A and Mayer E 1987 *J. Phys. Chem.* **91** 503
[32] Mishima O 1996 *Nature* **384** 546
[33] Kanno H, Speedy R J and Angell C A 1975 *Science* **189** 881
[34] Tombari E, Ferrari C, Salvetti G and Johari G P 1999 *J. Chem. Phys.* **111** 3115
[35] Krämer B, Hübner O, Vortisch H, Wötse L, Leisner T, Schwell M, Rühl E and Baumgärtel H 1999 *J. Chem. Phys.* **111** 6521
[36] Krämer B, Schwell M, Hübner O, Vortisch H, Leisner T, Rühl E, Baumgärtel H and Wöste L 1996 *Ber. Bunsenges. Phys. Chem.* **100** 1911
[37] Sassen K, Liou K N, Kinne S and Griffin M 1985 *Science* **227** 411
[38] Sassen K 1992 *Science* **257** 516
[39] Rosenfeld D and Woodley W L 2000 *Nature* **405** 440
[40] Koop T, Luo B, Tsias A and Peter T 2000 *Nature* **406** 611
[41] Pruppacher H R 1995 *J. Atmos. Sci.* **52** 1924
[42] Baker M B 1997 *Science* **276** 1072
[43] Bartell L S and Huang J 1994 *J. Phys. Chem.* **98** 7455
[44] Huang J and Bartell L S 1995 *J. Phys. Chem.* **99** 3924
[45] Wyslouzil B E, Cheung J L, Wilemski G and Strey R 1997 *Phys. Rev. Lett.* **79** 431
[46] Streletzky K A, Zvinevich Y, Wyslouzil B E and Strey R 2002 *J. Chem. Phys.* **116** 4058
[47] Heath C H, Streletzky K, Wyslouzil B E, Wölk J and Strey R 2002 *J. Chem. Phys.* **117** 6176

[48] Heath C H, Streletzky K A, Wyslouzil B E, Wölk J and Strey R 2003 *J. Chem. Phys.* **118** 5465
[49] Smith R S and Kay B D 1999 *Nature* **398** 788
[50] Johari G P 1998 *J. Phys. Chem.* B **102** 4711
[51] Jenniskens P, Banham S F, Blake D F and McCoustra 1997 *J. Chem. Phys.* **107** 1232
[52] Schufle J A 1965 *Chem. Indust.* **16** 690
[53] Schufle J A and Venugopalan M 1967 *J. Geophys. Res.* **72** 3271
[54] Zheleznyi B V 1969 *Russ. J. Phys. Chem.* **43** 1311
[55] Rasmussen D H and MacKenzie A P 1973 *J. Chem. Phys.* **59** 5003
[56] Kanno H and Angell C A 1980 *J. Chem. Phys.* **73** 1940
[57] Hare D E and Sorensen C M 1986 *J. Chem. Phys.* **84** 5085
[58] Hare D E and Sorensen C M 1987 *J. Chem. Phys.* **87** 4840
[59] Sotani T, Arabas J, Kubota H and Kijima M 2000 *High Temp.–High Pressures* **32** 433
[60] Speedy R J and Angell C A 1976 *J. Chem. Phys.* **65** 851
[61] Kanno H and Angell C A 1979 *J. Chem. Phys.* **70** 4008
[62] Xie Y, Ludwig K F, Morales G, Hare D E and Sorensen C M 1993 *Phys. Rev. Lett.* **71** 2050
[63] Angell C A and Kanno H 1976 *Science* **193** 1121
[64] Henderson S J and Speedy R J 1987 *J. Phys. Chem.* **91** 3062
[65] Anisimov M A, Voronel A V, Zaugolnikova N S and Ovodov G I 1972 *JETP Lett.* **15** 317
[66] Rasmussen D H, MacKenzie A P, Angell C A and Tucker J C 1973 *Science* **181** 342
[67] Angell C A, Shuppert J and Tucker J C 1973 *J. Phys. Chem.* **77** 3092
[68] Oguni M and Angell C A 1980 *J. Chem. Phys.* **73** 1948
[69] Angell C A, Oguni M and Sichina W J 1982 *J. Phys. Chem.* **86** 998
[70] Tombari E, Ferrari C and Salvetti G 1999 *Chem. Phys. Lett.* **300** 749
[71] Archer D G and Carter R W 2000 *J. Phys. Chem.* B **104** 8563
[72] Trinh E and Apfel R E 1978 *J. Acoust. Soc. Am.* **63** 777
[73] Trinh E and Apfel R E 1978 *J. Chem. Phys.* **69** 4245
[74] Trinh E and Apfel R E 1980 *J. Chem. Phys.* **72** 6731
[75] Petitet J P, Tufeu R and Le Neindre B 1983 *Int. J. Thermophys.* **4** 35
[76] Rouch J, Lai C C and Chen S H 1976 *J. Chem. Phys.* **65** 4016
[77] Teixeira J and Leblond J 1978 *J. Physique Lett.* **39** L83
[78] Conde O, Teixeira J and Papon P 1982 *J. Chem. Phys.* **76** 3747
[79] Bacri J-C and Rajaonarison R 1979 *J. Physique Lett.* **40** L403
[80] Magazú S, Maisano G, Majolino D, Mallamace F, Migliardo P, Aliotta F and Vasi C 1989 *J. Phys. Chem.* **93** 942
[81] Cunsolo A and Nardone M 1996 *J. Chem. Phys.* **105** 3911
[82] Liao C Y, Chen S H and Sette F 2000 *Phys. Rev.* E **61** 1518
[83] Rahman A and Stillinger F H 1974 *Phys. Rev.* A **20** 368
[84] Teixeira J, Bellissent-Funel M C, Chen S H and Dorner B 1985 *Phys. Rev. Lett.* **54** 2681
[85] Sette F, Ruocco G, Krisch M, Bergmann U, Masciovecchio C, Mazzacurati V, Signorelli G and Verbeni R 1995 *Phys. Rev. Lett.* **75** 850
[86] Ruocco G, Sette F, Bergmann U, Krisch M, Masciovecchio C, Mazzacurati V, Signorelli G and Verbeni R 1996 *Nature* **379** 521
[87] Sette F, Ruocco G, Krisch M, Masciovecchio C, Verbeni R and Bergmann U 1996 *Phys. Rev. Lett.* **77** 83
[88] Krisch M, Loubeyre P, Ruocco G, Sette F, Cunsolo A, D'Astuto M, LeToullec R, Lorenzen M, Mermet A, Monaco G and Verbeni R 2002 *Phys. Rev. Lett.* **89** 125502
[89] Cunsolo A, Ruocco G, Sette F, Masciovecchio C, Mermet A, Monaco G, Sampoli M and Verbeni R 1999 *Phys. Rev. Lett.* **82** 775
[90] Balucani U, Ruocco G, Torcini A and Vallauri R 1993 *Phys. Rev.* E **47** 1677
[91] Sciortino F and Sastry S 1994 *J. Chem. Phys.* **100** 3881
[92] Sampoli M, Ruocco G and Sette F 1997 *Phys. Rev. Lett.* **79** 1678
[93] Ruocco G and Sette F 1999 *J. Phys.: Condens. Matter* **11** R259
[94] Hasted J B and Shahidi M 1976 *Nature* **262** 777
[95] Hodge I M and Angell C A 1978 *J. Chem. Phys.* **68** 1363
[96] Das B K, Kraus G F, Siewick J T and Greer S C 1982 *Proc. 8th Symp. on Thermophysical Properties* vol 2, p 324
[97] Bertolini D, Cassettari M and Salvetti G 1982 *J. Chem. Phys.* **76** 3285
[98] Scheel K and Heuse W 1909 *Ann. Phys.* **29** 723
[99] Bottomley G A 1978 *Aust. J. Chem.* **31** 1177

[100] Douslin D R 1971 *J. Chem. Thermodyn.* **3** 197
[101] Kraus G F and Greer S C 1984 *J. Phys. Chem.* **88** 4781
[102] Young T F and Harkins W D 1928 *International Critical Tables of Numerical Data* vol 4, ed E Washburn (New York: McGraw-Hill) p 446
[103] Hacker P T 1951 *NACA Tech. Note* **2510** 1
[104] Floriano M A and Angell C A 1990 *J. Phys. Chem.* **94** 4199
[105] Trinh E H and Ohsaka K 1995 *Int. J. Thermophys.* **16** 545
[106] Pruppacher H R 1972 *J. Chem. Phys.* **56** 101
[107] Gillen K T, Douglass D C and Hoch M J R 1972 *J. Chem. Phys.* **57** 5117
[108] Angell C A, Finch E D, Woolf L A and Bach P 1976 *J. Chem. Phys.* **65** 3063
[109] Prielmeier F X, Lang E W, Speedy R J and Lüdemann H-D 1987 *Phys. Rev. Lett.* **59** 1128
[110] Harris K R and Newitt P J 1997 *J. Chem. Eng. Data* **42** 346
[111] Price W S, Ide H and Arata Y 1999 *J. Phys. Chem.* A **103** 448
[112] Price W S, Ide H, Arata Y and Söderman O 2000 *J. Phys. Chem.* B **104** 5874
[113] Arnold M R and Lüdemann H-D 2002 *Phys. Chem. Chem. Phys.* **4** 1581
[114] Smith R S, Dohnálek Z, Kimmel G A, Stevenson K P and Kay B D 2000 *Chem. Phys.* **258** 291
[115] Chen H-S, Teixeira J and Nicklow R 1982 *Phys. Rev.* A **26** 3477
[116] Teixeira J, Bellissent-Funel M-C, Chen S H and Dianoux A J 1985 *Phys. Rev.* A **31** 1913
[117] Smith R S, Huang C and Kay B D 1997 *J. Phys. Chem.* B **101** 6123
[118] Smith R S, Huang C, Wong E K L and Kay B D 1996 *Surf. Sci.* **367** L13
[119] White G and Twining R 1913 *Am. Chem. J.* **50** 380
[120] Hallett J 1963 *Proc. Phys. Soc.* **82** 1046
[121] Eicher L D and Zwolinski B J 1971 *J. Phys. Chem.* **75** 2016
[122] Osipov Y A, Zheleznyi B V and Bondarenko N F 1977 *Russ. J. Phys. Chem.* **51** 748
[123] Lang E and Lüdemann H-D 1977 *J. Chem. Phys.* **67** 718
[124] Lang E and Lüdemann H-D 1980 *Ber. Bunsenges. Phys. Chem.* **84** 462
[125] Lang E W and Lüdemann H-D 1981 *Ber. Bunsenges. Phys. Chem.* **85** 603
[126] Lang E W, Lüdemann H-D and Piculell L 1984 *J. Chem. Phys.* **81** 3820
[127] Lüdemann H-D 1990 *Ber. Bunsenges. Phys. Chem.* **94** 325
[128] Hindman J C, Svirmickas A and Wood M 1973 *J. Chem. Phys.* **59** 1517
[129] Hindman J C and Svirmickas A 1973 *J. Phys. Chem.* **77** 2487
[130] Rønne C, Thrane L, Åstrand P-O, Waalqvist A, Mikkelsen K V and Keiding S R 1997 *J. Chem. Phys.* **107** 5319
[131] Rønne C, Åstrand P-O and Keiding S 1999 *Phys. Rev. Lett.* **82** 2888
[132] Rønne C and Keiding S R 2002 *J. Mol. Liq.* **101** 199
[133] Burton E F and Oliver W F 1935 *Proc. R. Soc.* A **153** 166
[134] Sceats M G and Rice S A 1982 *Water—a Comprehensive Treatise* vol 7, ed F Franks (New York: Plenum) chapter 2
[135] Narten A H, Venkatesh C G and Rice S A 1976 *J. Chem. Phys.* **64** 1106
[136] Sack N J and Baragiola R A 1993 *Phys. Rev.* B **48** 9973
[137] Stirniman M J, Huang C, Smith R S, Joyce S A and Kay B D 1996 *J. Chem. Phys.* **105** 1295
[138] Stevenson K P, Kimmel G A, Dohnálek Z, Smith R S and Kay B D 1999 *Science* **283** 1505
[139] Dohnálek Z, Kimmel G A, Ciolli R L, Stevenson K P and Smith R S 2000 *J. Chem. Phys.* **112** 5932
[140] Kimmel G A, Stevenson K P, Dohnálek Z, Smith R S and Kay B D 2001 *J. Chem. Phys.* **114** 5284
[141] Safarik D J, Meyer R J and Mullins C B 2003 *J. Chem. Phys.* **118** 4660
[142] Brüggeller P and Mayer E 1980 *Nature* **288** 569
[143] Mayer E and Brüggeller P 1982 *Nature* **298** 715
[144] Dubochet J, Lepault J, Freeman R, Berriman J A and Homo J-C 1981 *J. Microsc.* **128** 219
[145] Dubochet J and McDowall A W 1981 *J. Microsc.* **124** RP3
[146] Mayer E 1985 *J. Appl. Phys.* **58** 663
[147] Bellissent-Funel M-C, Bosio L, Hallbrucker A, Mayer E and Sridi-Dorbez R 1992 *J. Chem. Phys.* **97** 1282
[148] Tulk C A, Klug D D, Branderhorst R, Sharpe P and Ripmeester J A 1998 *J. Chem. Phys.* **109** 8478
[149] Mishima O, Calvert L D and Whalley E 1984 *Nature* **310** 393
[150] Mishima O, Calvert L D and Whalley E 1985 *Nature* **314** 76
[151] Klug D D, Tulk C A, Svensson E C and Loong C-K 1999 *Phys. Rev. Lett.* **83** 2584
[152] Tse J S, Klug D D, Tulk C A, Swainson I, Svensson E C, Loong C-K, Shpakov V, Belosludov V R, Belosludov R V and Kawazoe Y 1999 *Nature* **400** 647
[153] Johari G P, Hallbrucker A and Mayer E 1996 *Science* **273** 90

[154] Mishima O and Suzuki Y 2001 *J. Chem. Phys.* **115** 4199
[155] Loerting T, Salzmann C, Kohl I, Mayer E and Hallbrucker A 2001 *Phys. Chem. Chem. Phys.* **3** 5355
[156] Ghormley J A and Hochanadel C J 1971 *Science* **171** 62
[157] Handa Y P and Klug D D 1988 *J. Phys. Chem.* **92** 3323
[158] Hallbrucker A, Mayer E and Johari G P 1989 *Phil. Mag.* B **60** 179
[159] Johari G P, Hallbrucker A and Mayer E 1990 *J. Chem. Phys.* **92** 6742
[160] Speedy R J, Debenedetti P G, Smith R S, Huang C and Kay B D 1996 *J. Chem. Phys.* **105** 240
[161] Fisher M and Devlin J P 1995 *J. Phys. Chem.* **99** 11584
[162] Johari G P 2002 *J. Chem. Phys.* **116** 8067
[163] Johari G P 2003 *J. Chem. Phys.* **119** 2935
[164] Tse J S and Klein M L 1987 *Phys. Rev. Lett.* **58** 1672
[165] Tse J S 1992 *J. Chem. Phys.* **96** 5482
[166] Finney J L, Hallbrucker A, Kohl I, Soper A K and Bowron D T 2002 *Phys. Rev. Lett.* **88** 225503
[167] Hemley R J, Chen L C and Mao H K 1989 *Nature* **338** 638
[168] Bizid A, Bosio L, Defrain A and Oumezzine M 1987 *J. Chem. Phys.* **87** 2225
[169] Floriano M A, Whalley E, Svensson E C and Sears V F 1986 *Phys. Rev. Lett.* **57** 3062
[170] Bellissent-Funel M-C, Teixeira J and Bosio L 1987 *J. Chem. Phys.* **87** 2231
[171] Klotz S, Hamel G, Loveday J S, Nelmes R J, Guthrie M and Soper A K 2002 *Phys. Rev. Lett.* **89** 285502
[172] Mishima O 1994 *J. Chem. Phys.* **100** 5910
[173] Handa Y P, Mishima O and Whalley E 1986 *J. Chem. Phys.* **84** 2766
[174] Floriano M A, Handa Y P, Klug D D and Whalley E 1989 *J. Chem. Phys.* **91** 7187
[175] Whalley E, Klug D D and Handa Y P 1989 *Nature* **342** 782
[176] Johari G P 1995 *J. Chem. Phys.* **102** 6224
[177] Mishima O, Takemura K and Aoki K 1991 *Science* **254** 406
[178] Mishima O and Suzuki Y 2002 *Nature* **419** 599
[179] Koza M M, Schober H, Fischer H E, Hansen T and Fujara F 2003 *J. Phys.: Condens. Matter* **15** 321
[180] Tulk C A, Benmore C J, Urquidi J, Klug D D, Neuefeind J, Tomberli B and Egelstaff P A 2002 *Science* **297** 1320
[181] Brazhkin V V, Gromnitskaya E L, Stal'gorova O V and Lyapin A G 1998 *Rev. High Pressure Sci. Technol.* **7** 1129
[182] Stal'gorova O V, Gromnitskaya E L, Brazhkin V V and Lyapin A G 1999 *JETP Lett.* **69** 694
[183] Finney J L, Bowron D T, Soper A K, Loerting T, Mayer E and Hallbrucker A 2002 *Phys. Rev. Lett.* **89** 205503
[184] Speedy R J 1982 *J. Phys. Chem.* **86** 982
[185] D'Antonio M C and Debenedetti P G 1987 *J. Chem. Phys.* **86** 2229
[186] Debenedetti P G and D'Antonio M C 1988 *AIChE J.* **34** 447
[187] Sastry S, Sciortino F and Stanley H E 1993 *J. Chem. Phys.* **98** 9863
[188] Sasai M 1993 *Bull. Chem. Soc. Japan* **66** 3362
[189] Borick S S, Debenedetti P G and Sastry S 1995 *J. Phys. Chem.* **99** 3781
[190] Debenedetti P G, Raghavan V S and Borick S S 1991 *J. Phys. Chem.* **95** 4540
[191] Speedy R J 1982 *J. Phys. Chem.* **86** 3002
[192] Sengers J V and Levelt-Sengers J M H 1978 *Progress in Liquid Physics* ed C A Croxton (Chichester: Wiley) p 103
[193] Poole P H, Sciortino F, Essmann U and Stanley H E 1992 *Nature* **360** 324
[194] Angell C A 1995 *Science* **267** 1924
[195] Poole P H, Grande T, Angell C A and McMillan P F 1997 *Science* **275** 322
[196] Bellissent-Funel M-C 1998 *Europhys. Lett.* **42** 161
[197] Bellissent-Funel M-C and Bosio L 1995 *J. Chem. Phys.* **102** 3727
[198] Starr F W, Bellissent-Funel M-C and Stanley H E 1999 *Phys. Rev.* E **60** 1084
[199] Stillinger F H and Rahman A 1974 *J. Chem. Phys.* **60** 1545
[200] Poole P H, Sciortino F, Essmann U and Stanley H E 1993 *Phys. Rev.* E **48** 3799
[201] Jorgensen W L, Chandrasekhar J, Madura J D, Impey R W and Klein M L 1983 *J. Chem. Phys.* **79** 926
[202] Poole P H, Essmann U, Sciortino F and Stanley H E 1993 *Phys. Rev.* E **48** 4605
[203] Mishima O and Stanley H E 1998 *Nature* **392** 164
[204] Mishima O 2000 *Phys. Rev. Lett.* **85** 334
[205] Roberts C J, Panagiotopoulos A Z and Debenedetti P G 1996 *Phys. Rev. Lett.* **77** 4386
[206] Roberts C J and Debenedetti P G 1996 *J. Chem. Phys.* **105** 658
[207] Harrington S, Zhang R, Poole P H, Sciortino F and Stanley H E 1997 *Phys. Rev. Lett.* **78** 2409
[208] Sciortino F, Poole P H, Essmann U and Stanley H E 1997 *Phys. Rev.* E **55** 727

[209] Yamada M, Stanley H E and Sciortino F 2003 *Phys. Rev.* E **67** 010202
[210] Mahoney M W and Jorgensen W L 2000 *J. Chem. Phys.* **112** 8910
[211] Yamada M, Mossa S, Stanley H E and Sciortino F 2002 *Phys. Rev. Lett.* **88** 195701
[212] Brovchenko I, Geiger A and Oleinikova A 2003 *J. Chem. Phys.* **118** 9473
[213] Hansen J-P and Verlet L 1969 *Phys. Rev.* **184** 151
[214] Corti D S and Debenedetti P G 1994 *Chem. Eng. Sci.* **49** 2717
[215] Scala A, Starr F W, La Nave E, Stanley H E and Sciortino F 2000 *Phys. Rev.* E **62** 8016
[216] Berendsen H J C, Grigera J R and Straatsma T P 1987 *J. Phys. Chem.* **91** 6269
[217] Rosenfeld Y and Tarazona P 1998 *Mol. Phys.* **95** 141
[218] Tanaka H 1996 *Nature* **380** 328
[219] Tanaka H 1996 *J. Chem. Phys.* **105** 5099
[220] Poole P H, Sciortino F, Grande T, Stanley H E and Angell C A 1994 *Phys. Rev. Lett.* **73** 1632
[221] Truskett T M, Debenedetti P G, Sastry S and Torquato S 1999 *J. Chem. Phys.* **111** 2647
[222] Jeffrey C A and Austin P H 1999 *J. Chem. Phys.* **110** 484
[223] Franzese G and Stanley H E 2002 *J. Phys.: Condens. Matter* **14** 2201
[224] Truskett T M and Dill K A 2002 *J. Chem. Phys.* **117** 5101
[225] Truskett T M and Dill K A 2002 *J. Phys. Chem.* B **106** 11829
[226] Malescio G, Franzese G, Pellicane G, Skibinsky A, Buldyrev S V and Stanley H E 2002 *J. Phys.: Condens. Matter* **14** 2193
[227] Hemmer P C and Stell G 1970 *Phys. Rev. Lett.* **24** 1284
[228] Stell G and Hemmer P C 1972 *J. Chem. Phys.* **56** 4274
[229] Kincaid J M, Stell G and Hall C K 1976 *J. Chem. Phys.* **65** 2161
[230] Kincaid J M, Stell G and Goldmark E 1976 *J. Chem. Phys.* **65** 2172
[231] Kincaid J M and Stell G 1977 *J. Chem. Phys.* **67** 420
[232] Kincaid J M and Stell G 1978 *Phys. Lett.* A **65** 131
[233] Sadr-Lahijany M R, Scala A, Buldyrev S V and Stanley H E 1998 *Phys. Rev. Lett.* **81** 4895
[234] Franzese G, Malescio G, Skibinsky A, Buldyrev S V and Stanley H E 2001 *Nature* **409** 692
[235] Malescio G and Pellicane G 2001 *Phys. Rev.* E **63** 020501(R)
[236] Scala A, Sadr-Lahijany M R, Giovambattista N, Buldyrev S and Stanley H E 2001 *Phys. Rev.* E **63** 041202
[237] Jagla E A 1998 *Phys. Rev.* E **58** 1478
[238] Jagla E A 1999 *J. Phys.: Condens. Matter* **11** 10251
[239] Jagla E A 1999 *J. Chem. Phys.* **111** 8980
[240] Jagla E A 2001 *Phys. Rev.* E **63** 061509
[241] Jagla E A 2001 *Phys. Rev.* E **63** 061501
[242] Mon K K, Ashcroft N W and Chester G V 1979 *Phys. Rev.* B **19** 5103
[243] Cummings P T and Stell G 1981 *Mol. Phys.* **43** 1267
[244] Moynihan C T 1997 *Mater. Res. Soc. Symp. Proc.* **455** 411
[245] Ponyatovsky E G, Sinand V V and Pozdnyakova T A 1994 *JETP Lett.* **60** 360
[246] Ponyatovsky E G, Sinitsyn V V and Pozdnyakova T A 1998 *J. Chem. Phys.* **109** 2413
[247] Ponyatovsky E G and Sinitsyn V V 1999 *Physica* B **265** 121
[248] Tanaka H 1998 *Phys. Rev. Lett.* **80** 5750
[249] Tanaka H 1999 *J. Phys.: Condens. Matter* **11** L159
[250] Tanaka H 2000 *J. Chem. Phys.* **112** 799
[251] Tanaka H 2000 *Europhys. Lett.* **50** 340
[252] Tanaka H 2000 *Phys. Rev.* E **62** 6968
[253] Geiger A and Stanley H E 1982 *Phys. Rev. Lett.* **49** 1749
[254] Tanaka H 1998 *Phys. Rev. Lett.* **80** 113
[255] Shiratani E and Sasai M 1998 *J. Chem. Phys.* **108** 3264
[256] Sasai M 2000 *Physica* A **285** 315
[257] Debenedetti P G 1998 *Nature* **392** 127
[258] Rebelo L P N, Debenedetti P G and Sastry S 1998 *J. Chem. Phys.* **109** 626
[259] La Nave E, Sastry S, Sciortino F and Tartaglia P 1999 *Phys. Rev.* E **59** 6348
[260] Stanley H E 1979 *J. Phys. A: Math. Gen.* **12** L329
[261] Blumberg R L, Shlifer G and Stanley H E 1980 *J. Phys. A: Math. Gen.* **13** L147
[262] Sasai M 1990 *J. Chem. Phys.* **93** 7329
[263] Born M and Huang K 1954 *Dynamical Theory of Crystal Lattices* (Oxford: Clarendon)
[264] Lindemann F A 1910 *Z. Phys.* **11** 609
[265] Speedy R J 1992 *J. Phys. Chem.* **96** 2322

[266] Sceats M S and Rice S A 1980 *J. Chem. Phys.* **72** 3260
[267] Angell C A 1993 *J. Phys. Chem.* **97** 6339
[268] Shpakov V P, Rodger P M, Tse J S, Klug D D and Belosludov V R 2002 *Phys. Rev. Lett.* **88** 155502
[269] Kiselev S B 1999 *Physica* A **269** 252
[270] Kiselev S B and Ely J F 2001 *Physica* A **299** 357
[271] Kiselev S B and Ely J F 2002 *J. Chem. Phys.* **116** 5657
[272] Kiselev S B and Ely J F 2003 *J. Chem. Phys.* **118** 680
[273] Gallo P, Sciortino F, Tartaglia P and Chen S-H 1996 *Phys. Rev. Lett.* **76** 2730
[274] Sciortino F, Gallo P, Tartaglia P and Chen H-S 1996 *Phys. Rev.* E **54** 6331
[275] Sciortino F, Fabbian L, Vhen H-S and Tartaglia P 1997 *Phys. Rev.* E **56** 5397
[276] Sciortino F 2000 *Chem. Phys.* **258** 307
[277] Götze W and Sjögren L 1992 *Rep. Prog. Phys.* **55** 241
[278] Starr F W, Harrington S, Sciortino F and Stanley H E 1999 *Phys. Rev. Lett.* **82** 3629
[279] Starr F W, Sciortino F and Stanley H E 1999 *Phys. Rev.* E **60** 6757
[280] Fabbian L, Sciortino F, Thiery F and Tartaglia P 1998 *Phys. Rev.* E **57** 1485
[281] Fabbian L, Latz A, Schilling R, Sciortino F, Tartaglia P and Thies C 1999 *Phys. Rev.* E **60** 5768
[282] Fabbian L, Latz A, Schilling R, Sciortino F, Tartaglia P and Thies C 2000 *Phys. Rev.* E **62** 2388
[283] Patschek D and Geiger A 1999 *J. Phys. Chem.* B **103** 4139
[284] Starr F W, Angell C A and Stanley H E 2003 *Physica* A **323** 51
[285] Adam G and Gibbs J H 1965 *J. Chem. Phys.* **43** 139
[286] Richert R and Angell C A 1998 *J. Chem. Phys.* **108** 9016
[287] Stillinger F H 1995 *Science* **267** 1935
[288] Sastry S 2001 *Nature* **409** 164
[289] Sciortino F, Kob W and Tartaglia P 1999 *Phys. Rev. Lett.* **83** 3214
[290] Pauling L 1935 *J. Am. Chem. Soc.* **57** 2680
[291] Ito K, Moynihan C T and Angell C A 1999 *Nature* **398** 492
[292] Scala A, Starr F W, La Nave E, Sciortino F and Stanley H E 2000 *Nature* **406** 166
[293] Debenedetti P G and Stillinger F H 2001 *Nature* **410** 259
[294] La Nave E, Scala A, Starr F W, Sciortino F and Stanley H E 2000 *Phys. Rev. Lett.* **84** 4605
[295] Giovambattista N, Buldyrev S V, Starr F W and Stanley H E 2003 *Phys. Rev. Lett.* **90** 085506
[296] Sciortino F, La Nave E, Scala A, Stanley H E and Starr F W 2002 *Eur. Phys. J.* E **9** 233
[297] Katayama Y, Mizutani T, Utsumi W, Shimomura O, Yamakata M and Funakoshi K-i 2000 *Nature* **403** 170
[298] Brazhkin V, Buldyrev S V, Ryzhov V N and Stanley H E (ed) 2002 New kinds of phase transitions: transformations in disordered substances *Proc. NATO Advanced Research Workshop (Volga River, 2002)* (Dordrecht: Kluwer)
[299] Lebowitz J L and Penrose O 1966 *J. Math. Phys.* **7** 98
[300] Penrose O and Lebowitz J L 1971 *J. Stat. Phys.* **3** 211
[301] Kivelson D and Reiss H 1999 *J. Phys. Chem.* B **103** 8337
[302] Corti D S and Debenedetti P G 1998 *Phys. Rev.* E **57** 4211
[303] Franks F and Hatley R H M 1991 *Pure Appl. Chem.* **63** 1367
[304] Franks F 1985 *Biophysics and Biochemistry at Low Temperatures* (Cambridge: Cambridge University Press)
[305] Jenniskens P and Blake D F 1994 *Science* **265** 753
[306] Jenniskens P, Blake D F, Wilson M A and Pohorille A 1995 *Astrophys. J.* **455** 389
[307] Jenniskens P and Blake D F 1996 *Astrophys. J.* **473** 1104
[308] Cocks F H, Klenk P A, Watkins S A, Simmons W N, Cocks J C, Cocks E E and Sussingham J C 2002 *Icarus* **160** 386
[309] Roberts C J and Debenedetti P G 2002 *AIChE J.* **48** 1140
[310] Fine R A and Millero F J 1975 *J. Chem. Phys.* **63** 89
[311] Kell G S 1975 *J. Chem. Eng. Data* **20** 97
[312] Kell G S 1967 *J. Chem. Eng. Data* **12** 66
[313] Emmett R T and Millero F J 1975 *J. Chem. Eng. Data* **20** 351
[314] Onsager L and Runnels L K 1969 *J. Chem. Phys.* **50** 1089
[315] Goto K, Hondoh T and Higashi A 1986 *Japan. J. Appl. Phys.* **25** 351
[316] Angell C A 1988 *Nature* **331** 206